FISEVIER

Contents lists available at ScienceDirect

Quaternary Science Reviews

journal homepage: www.elsevier.com/locate/quascirev



Quaternary diatoms and palaeoenvironments of the Koora Plain, southern Kenya rift



Veronica Muiruri ^a, R. Bernhart Owen ^{b,*}, Richard Potts ^c, Alan L. Deino ^d, Anna K. Behrensmeyer ^e, Simon Riedl ^f, Nathan Rabideaux ^g, Emily J. Beverly ^h, Robin W. Renaut ⁱ, Jessica W. Moerman ^c, Daniel Deocampo ^j, J. Tyler Faith ^{k, l}, Anders Noren ^m, Andrew S. Cohen ⁿ, Kristina Brady Shannon ^m, René Dommain ^{c, f}

- ^a Department of Earth Sciences, Palynology and Paleobotany Section, National Museums of Kenya, Nairobi, Kenya
- ^b Department of Geography, Hong Kong Baptist University, Kowloon Tong, Hong Kong, China
- ^c Human Origins Program, National Museum of Natural History, Smithsonian Institution, Washington, DC, 20013, USA
- ^d Berkeley Geochronology Center, Ridge Road, Berkeley, CA, 94709, USA
- e Department of Paleobiology, National Museum of Natural History, Smithsonian Institution, Washington, DC, 20013, USA
- ^f Institute of Geosciences, University of Potsdam, 14476, Potsdam, Germany
- g Department of Chemistry, Rutgers University, Newark, NJ, 07102, USA
- ^h Department of Earth and Atmospheric Sciences, University of Houston, TX, 77204, USA
- ⁱ Department of Geological Sciences, University of Saskatchewan, Saskatoon, SK S7N 5E2, Canada
- ^j Department of Geosciences, Georgia State University, Atlanta, GA, 30302, USA
- k Natural History Museum of Utah, University of Utah, Salt Lake City, UT, 84108, USA
- ¹ Department of Anthropology, University of Utah, Salt Lake City, UT, 84112, USA
- ^m Continental Scientific Drilling Coordination Office and LacCore Facility, Dept of Earth and Environmental Sciences, University of Minnesota, Minneapolis, MN, 55455, USA
- ⁿ Department of Geosciences, University of Arizona, Tucson, AZ, 85721, USA

ARTICLE INFO

Article history: Received 28 April 2021 Received in revised form 20 July 2021 Accepted 21 July 2021 Available online 4 August 2021

Handling Editor: P Rioual

Keywords: Pleistocene Palaeolimnology Diatoms Lake levels Hominins Kenya Rift Africa

ABSTRACT

The Koora Basin (south Kenya Rift) preserves a continental, tropical, one-million-year record of environmental change driven by global climate, regional tectonism and volcanism. Diatom-based reconstructions from Olorgesailie Drilling Project (ODP) cores indicate lakes that expanded and contracted with conductivities ranging between ~200 and > 25,000 $\mu S.cm^{-1}$ and pH of 7.9–11.2. Benthic and planktonic diatoms document mostly shallow fresh water between 1 Ma and 870 ka with deeper freshwater lakes from 870 to 470 ka. After the Mid-Brunhes Event at about 430 ka, diatoms record many transgression-regression cycles with both freshwater and saline-alkaline lakes present. Palaeosols also indicate episodes of desiccation and lower water tables. Carbonates and zeolites are present in younger sediments, especially after 400 ka. Many high-lake-level stages correlate with low values in ocean benthic δ^{18} O stack data. Most, but not all, low lake levels occurred during higher δ^{18} O MIS intervals, suggesting tectonic and/or volcanic events, in addition to climatic forcing, influenced the drainage, outlet heights and accommodation space.

The 870–470 ka period of deeper freshwater lakes at Koora correlates well with the neighbouring Lake Magadi pollen record that suggests generally wetter conditions at this time. Wet-dry cycles after 470 ka at Koora developed when the Magadi record indicates a change towards drier conditions, but with many wetter intervals. High lake level periods at Koora also correlate with phases of diatom-inferred flooding at Magadi. Outcrops north of Koora also document several large lakes during deposition of parts of the Olorgesailie Formation prior to ~500 ka. The Koora environmental history helps to fill an environmental gap (500–320 ka) encompassing critical changes in hominin lithic technology caused by a hiatus at

E-mail address: owen@hkbu.edu.hk (R.B. Owen).

^{*} Corresponding author.

Olorgesailie. During the first part of this interval (470–390 ka), Koora was occupied by a shallow alkaline lake, suggesting relatively dry conditions. The second part (390–320 ka) was characterised by fluctuating deeper lakes that imply greater variability and wetter conditions. Subsequently, both the Olorgesailie and Koora records indicate variable environments.

© 2021 Elsevier Ltd. All rights reserved.

1. Introduction

Recent discoveries have pushed back the origins of *Homo sapiens* to about 315 ka (Hublin et al., 2017), and our history extends much deeper in time through hominin genera such as Homo, Australopithecus, Ororrin and Sahelanthropus. Our physical and cultural evolution has involved bipedalism, changes in body morphology, brain expansion and the development of a variety of stone tools. Palaeoanthropological research on these aspects of our ancestry has also stimulated an interest in environmental change as a factor in human evolution (deMenocal, 1995; Potts, 1998; Potts and Faith, 2015; Campisano et al., 2017; Faith et al., 2021). Potts (2013), for example, summarised how evolutionary events have variously been attributed to shifts, such as increasing aridity and changing environmental variability. A variety of controls have been suggested to explain the forces that drove environmental change in regional climate, including tectonism, northern hemisphere glaciation, ocean temperatures and the impact of variations in Earth's eccentricity, obliquity and precession (deMenocal, 2004; Sepulchre et al., 2006; Potts and Faith, 2015).

Research into the relationships between hominins and climateenvironment drivers of evolutionary change has relied on studies of outcrops that contain fossil hominins or their stone tools (Owen et al., 2008a; Potts et al., 2018). Sedimentary records at these locations are commonly patchy in space and time so that important periods in hominin evolution tend to be associated with discontinuous environmental records (Cohen et al., 2009). Additional difficulties arise from a scale-related mismatch between finelyresolved core-based records from distant marine locations, which average data over large regions (deMenocal, 1995), and the temporally-less-detailed basin-scale archives of hominin evolution (Campisano et al., 2017; Faith et al., 2021). The need for improved environmental histories that can be more closely tied to hominins in East Africa led to the development of three projects: the Olorgesailie Drilling Project (ODP), the Hominin Sites and Paleolakes Drilling Project (HSPDP) and the Olduvai Gorge Coring Project (OGCP) (Potts et al., 2020; Cohen et al., 2016; Owen et al., 2018; Njau et al., 2020).

An aeromagnetic survey by Wohlenberg and Bhatt (1972) showed that a thick sequence of sediments underlies the Koora Plain in the south Kenya Rift. These middle-to-late Pleistocene deposits were drilled by the ODP, resulting in two cores (ODP-OLO12-1A and -3A, Fig. 1A). In addition, the HSPDP team recovered two cores from Lake Magadi (Cohen et al., 2016; Campisano et al., 2017; Owen et al., 2018, 2019). Both sets of cores encompass sedimentary records for the last one-million-years near to the Olorgesailie Basin, which hosts abundant Acheulean and Middle Stone Age (MSA) tools (Deino and Potts, 1990; Brooks et al., 2018). However, despite the abundant artefacts at Olorgesailie, the environmental record there has numerous stratigraphic breaks related erosion surfaces, non-deposition and pedogenesis (Behrensmeyer et al., 2002). Notably, a major hiatus separates lacustrine, fluvial and terrestrial deposits of the Olorgesailie Formation (~1200-500 ka) from overlying middle to late Pleistocene cut-and-fill sediments of the Oltululei Formation (320-36 ka;

Behrensmeyer et al., 2018).

The research reported here is based on interpretation of a 139m-long core (ODP-OLO12-1A) that penetrated ~ 4 m into a basal trachyte (Potts et al., 2020). The core is located on the western Koora Plain and ranges in age between ~1084 and 83.5 ka. Deino et al. (2019) previously presented the chronostratigraphy and Bayesian age-model of this core and Potts et al. (2020) provided a synthesis of diatom, geochemical, phytolith and other proxy data as a background to their examination of hominin evolution and resource usage. This study develops a detailed diatom record and palaeoenvironmental history for the Koora palaeolake sediments. Our aim is to 1) document a diatom stratigraphy for the ODP-OLO12-1A core, 2) provide a palaeoenvironmental interpretation that helps to fill gaps associated with a major erosional hiatus (500-320 ka) and cut-and-fill cycles (320-97 ka) in the Olorgesailie Basin, and 3) compare the Koora palaeolake history with other parts of the southern Kenya Rift and global climate trends.

2. Geological setting

Fig. 1A and B shows the topographic and geological setting together with the location of modern lakes and their likely maximum Quaternary extent. The modern rift floor slopes southwards from about 1000 m above sea level (asl) near Olorgesailie through the Koora Graben (west of Mt. Olorgesailie) to the Koora Plain and on to the Siriata Graben (Fig. 1A) where diatomites and silts crop out. The Koora Plain lacks surface exposures, but Parkinson (1914) described ~14 feet of red clay resting on laminated silts, clays, diatomites, tuffs, pumice and shells (Planorbis pfeifferi, P. gibbons, Isodora contorta) in a 100-foot shaft dug in the early twentieth century. Busk (1939) subsequently marked an "old lake" south of Mt. Olorgesailie on his sketch of the rift valley. Although today's drainage basins in the southern Kenya rift have limited interconnections, Baker (1958), Crossley (1976) and Marsden (1979) noted undated terraces, overflow channels and palaeodrainage from the Koora Basin to Lake Magadi. Washbourn-Kamau (1977) and Baker and Mitchell (1976) reported a poorly dated late Quaternary megaflood that traversed the region from Lake Naivasha to Olorgesailie and possibly farther to Lake Magadi (Fig. 1A).

Over the last million years the rift floor has been cut by numerous north-south trending faults that have produced horsts and grabens, tilt blocks and fault ramps that define the many sedimentary basins in the region (Baker, 1958, 1986, 1986; Muirhead and Kattenhorn, 2018; Owen et al., 2019). Northwest—southeast lineaments rooted in subvolcanic basement (Fig. 1B) also control the location of cinder cones, hot spring groups and the southwestern margin of the Koora Plain.

Environmental change over the last million years is also represented in outcrops in the Magadi Basin, 10–15 km west of Koora. Several authors have described the discontinuous succession (Baker, 1958; Surdam and Eugster, 1976; Eugster, 1980; Behr, 2002; Owen et al., 2019), which includes a basal lacustrine limestone overlain by zeolitic lacustrine silt of the Oloronga Formation (~780–300 ka). These deposits were tilted and eroded and then

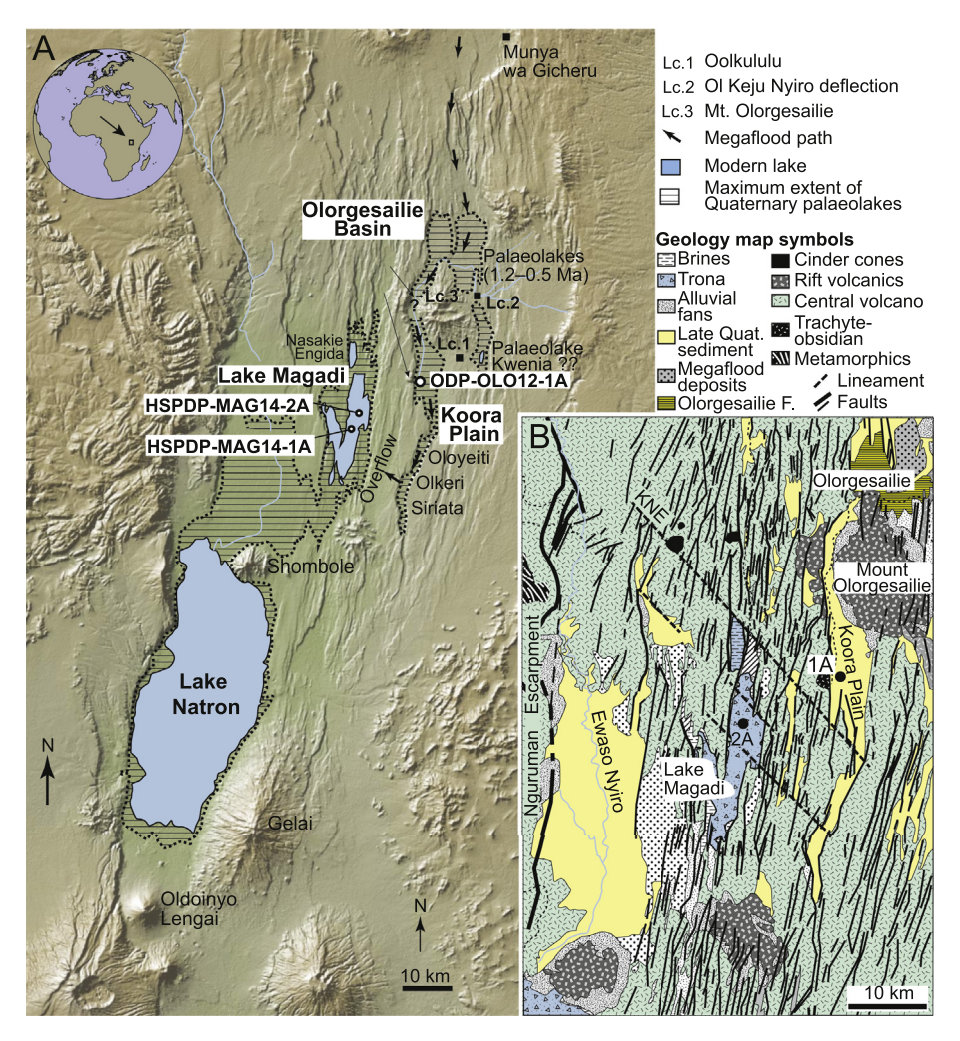


Fig. 1. Geography and geology of the Koora Plain and adjacent basins. A) Modern topography and maximum Quaternary extent of palaeolakes. After Hillaire-Marcel and Casanova (1987), Marsden (1979) and Behrensmeyer et al. (2002, 2018). Other grabens also contained lakes but are poorly understood. Basemap from GeoMapApp. B) Regional geology, after Owen et al. (2019) and Guth (2014). Note NW-SE photolineaments with the KNE (Kisamis-Nasikie Engida) tectonic alignment including the Kisamis cinder cone, hot springs and the southern graben termination of the Koora Plain.

capped by calcrete (Felske, 2016) prior to deposition of the "Green Beds" (lacustrine zeolitic silt and chert), dated at 191.8—40 ka (Goetz and Hillaire-Marcel, 1992; Behr, 2002). The late Pleistocene to Holocene High Magadi Beds (lacustrine zeolitic silt, clay, ash, magadiite) are overlain by Holocene trona (Eugster, 1980). Owen et al. (2018) and Muiruri et al. (2021) described the geochemistry, mineralogy, diatoms and pollen content of a 194-m Lake Magadi core (HSPDP-MAG14-2A; Fig. 1A) that penetrated to trachyte dated at 1.08 Ma (Fig. 1B), and which provides an informative, temporally synchronous comparison for the data reported here.

3. Materials and methods

Differential GPS elevations from the coring locations were obtained using a Leica Viva system, which were post-processed using our own base station data and data from the RCMN ("Regional Centre for Mapping", Nairobi) station. Structure-from-motion elevation data were collected in July 2016 and calibrated with the dGPS elevations. Basin-scale hypsometry was determined from the SRTM-30 m digital elevation model.

Core ODP-OLO12-1A was drilled on the Koora Plain (Fig. 2) at an elevation of 845 m and penetrated to a depth of 166.14 m through middle to late Pleistocene sediments and into Magadi Trachyte

flood lava. The upper 27 m was augered and the lower 139 m was cored (94% recovery) with 27 gaps resulting from no recovery, sediment loss or drilling disturbance. The core was sent to the US National Lacustrine Core Facility (LacCore) at the University of Minnesota (Minneapolis, USA) where it was logged, sampled and permanently archived. Loose homogenised samples were collected for diatom analyses at 1 m intervals from the upper augered part of the sequence. Core samples for diatom analyses were collected at regular 48 cm intervals, with additional samples related to lithological changes. After initial results were obtained, facies containing diatoms were further retrieved at 10 cm intervals, yielding a total of 600 samples for analysis.

Carbonate was removed from samples using dilute (10 %) HCl acid followed by rinsing with distilled water. Organic components were removed using H_2O_2 (Owen et al., 2008a). Known concentrations of silica microspheres (8 μ m diameter) were added in order to estimate diatom abundance (Battarbee and Kneen, 1982), followed by drying on to slides and mounting with naphrax®.

In most samples at least 400 diatoms were counted with a maximum count of 1602. Where there were too few valves, all diatoms were recorded. Individual diatoms were counted when more than half of a valve was present. The apices of slender fragmented taxa were counted and divided by two to estimate their abundance.

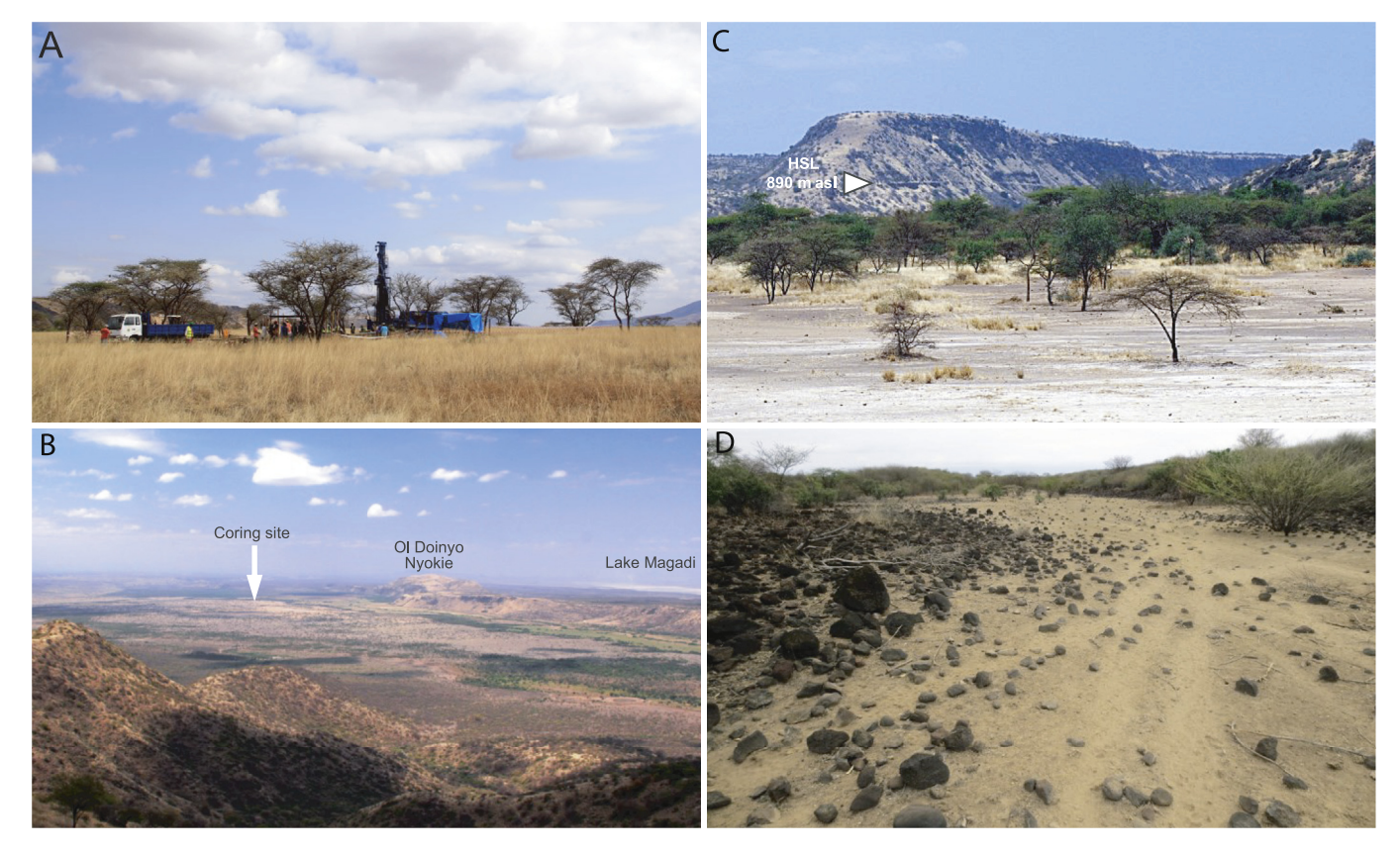


Fig. 2. The Koora Basin and coring site. A) ODP-OLO12-1A coring location, September 2012 (photo R. Dommain). B) View from Mount Olorgesailie over the Koora Plain and ODP core site. Ol Doinyo Nyokie volcano to the right cut by a north-south oriented fault. Lake Magadi far right with white trona (photo R. Dommain). C) Palaeoshoreline at 890 m on eastern paleolake margin indicates that tectonic activity has down-faulted the western horst blocks which, at 860 m, define the current basin margin. This palaeoshoreline is likely to represent a lake phase earlier than ~80 ka, as the geometry of the corresponding lake basin must have been different from today. As age control of this shoreline is not available, the temporal context of this lake level and the subsequent normal faulting remains speculative (photo S. Riedl). D) Cobble and boulder bars (left and right) formed by a flood that overtopped the southwestern bounding horst block of the Koora palaeolake (photo R.B. Owen). Note donkey trails for scale.

Taxonomic identifications were made at 1000 × magnification based on Gasse (1986) and Krammer and Lange-Bertalot (1986, 1988, 1991a, 1991b). Diatom identifications were confirmed using a Leo 1530 Field Emission Scanning Electron Microscope. Diatom nomenclature was also updated to the most recent accepted taxonomic names using Algaebase (Guiry and Guiry, 2021).

Stratigraphic diagrams were drafted using C2 software (Juggins, 2007) with taxa forming >10 % of the flora in at least one sample being included in order to reduce crowding in Figs. 4 and 5. This reduced the diatoms represented from 105 to 51 taxa with A. agassizii and its variety malayensis also merged in Fig. 4. Details of diatoms present at lower abundances are provided in full in supplementary Table S1 as both percentages and as counts. The selection process reduced the total count represented by the figures from 401,643 to 386,845. Taxa removed belonged to the genera Cymbella, Caloneis, Campylodiscus, Amphora, Halamphora, Achnanthes, Anomoeoneis, Luticola, Navicula, Sellaphora, Surirella, Iconella, Eunotia, Nizschia, Tabellaria, Terpsinoe, Pinnularia, Mastogloia and Stephanodiscus.

Correspondence Analysis (CA) and Agglomerative Hierarchical Clustering (AHC) were used to explore the relationships between diatoms. The CA was performed on 65 common taxa (\geq 3% in at least 2 samples or \geq 10% in at least 1 sample) using CANOCO 4.51 (ter Braak, 1986). Agglomerative Hierarchical Clustering, using Pearson Dissimilarity, was carried out with XLSTAT for EXCEL and was applied to 38 taxa that occurred regularly in the samples (\geq 5% in at least 3 samples or \geq 10% in at least 2 samples).

Electrical conductivity and pH reconstructions are based on

transfer functions and the 'Combined Salinity' dataset provided by the European Diatom Database (Battarbee et al., 1998) and used 'Locally-weighted Weighted Averaging' (LWWA) so that the data can be compared with diatom analyses by Owen et al. (2008a) at Olorgesailie. LWWA yields a local training set for each fossil sample using the 50 closest analogues defined by minimum chi-squared distance. Preference statistics suggested inverse deshrinking generated the better models for pH (RMSE_P = 0.36, r^2 = 0.69, Mean bias = 0.01, Max bias = 0.71) and conductivity (RMSE_P = 0.34, r^2 = 0.86, Mean bias = 0.02, Max bias = 0.76). Diatom habitats are based on the works of Gasse (1986, 1987), Gasse et al. (1995) and Zalat and Servant-Vildary (2007). The Simpson 1-D index was calculated using PAST 4.06 (Hammer et al., 2001) and ranges from 0 to 1 with low values representing equally present taxa and values of 1 indicating dominance by a single taxon.

4. Results

4.1. Chronology and sedimentology

The age model for core ODP-OLO12-1A is based on $21 \, ^{40} \text{Ar}/^{39} \text{Ar}$ dates from tephra, one $^{40} \text{Ar}/^{39} \text{Ar}$ date (1084 ka) for the underlying Magadi Trachyte and the position of the Brunhes-Matuyama Chron boundary. The Bayesian age-depth model is fully described by Deino et al. (2019). This model takes into account pauses in sedimentation related to palaeosol development, other hiatuses in sedimentation, and intervals of markedly increased sedimentation.

Table 1 summarises the characteristics of 22 major facies with

Table 1Major sedimentary facies in Core 1A. Terminology for diatomaceous sediments follows Owen et al. (2008a). See Fig. 3 for representative images.

Primary Lithologies	Facies code	Lithology, structure	Associated features and diatom content	Environment
F1. Massive subdiatomite.	Dm	Homogenous to vaguely bedded, white to pale yellow. Total silica up to 70 %. Diatom frustules abundant, together with clay and minor silt, sometimes bioturbated.	Thalassiosira and Cyclotella; sponge spicules/phytoliths present.	Shallow to deep lakes with low clastic inputs.
F2. Massive calcareous subdiatomite/ diatomaceous silt.		Homogeneous to vaguely bedded, diatom content variable, sometimes bioturbated. Carbonate variable, generally from 10 to 90%.	Aulacoseira spp. common, saline species (Thalassiosira/Cyclotella) common; sponge spicules/phytoliths present.	Shallow to moderately deep, saline to moderately saline lakes.
F3. Bedded subdiatomite and clayey/silty subdiatomite.	Db(a)	Diatomite beds alternate with clayey or silty diatomite. Deposits sometimes interbedded with pumice. May be calcareous (a).	Aulacoseira spp., particularly A. granulata, A. agassizii and A. granulata v. angustissima. T. faurii and P. ocellata in clay/silt.	Moderately deep to deep freshwater lake.
F4. Laminated diatomite and clay.	Dl	Similar to F3, but with mm-scale diatomite and clayey diatomite laminae.	A. granulata and A. agassizi dominant. Burrows present.	Deep freshwater lake.
F5. Diatomaceous silt/clayey silt/ sandy silt.	Zd/ Zcd Zsd	Massive to weakly bedded/laminated silts, clayey silts and sandy silts. Variable diatom content up to 70% of total components. Variable siliciclastics and volcanic glass. Variable carbonate content, mostly minor.	Mainly fresh to moderately saline diatoms. Varied benthic taxa common, especially <i>C. placentula</i> , <i>E. muelleri</i> , <i>C. elkab</i> , <i>N. frustulum</i> , <i>N. palea</i> ; phytoliths, sponge spicules.	Fresh to moderately saline shallow to moderately deep lakes and wetlands.
F6. Diatomaceous organic-rich clay/ silt.		Amorphous algal organic matter up to 40% together with variable diatom, siliciclastic and volcanic glass components. Organics sometimes in patches (as in image "F").		Shallow lacustrine.
F7. Silty clay with clay laminae (diatomaceous).	Czl(d)	Massive silty clay with intermittent clay-rich laminae. Clay dominant with secondary volcanic glass and siliciclastics. Clay laminae often drape over pumice and other clasts.	Diatoms rare with varied benthic floras (R. gibberula, N. palea common), phytoliths.	Lacustrine.
F8. Silt/clayey silt with carbonate nodules.	Za	Diatomaceous silts with vertically to subhorizontally oriented carbonate nodules. Horizontal and vertical rhizoliths may be present. Volcanic glass, siliciclastics variously present.	Diatoms very varied, including either benthic or planktonic species. Charcoal, phytoliths, amorphous algal matter variably present.	Pedogenically altered lake deposits.
F9. Clay with peds.		Non-laminated clay with peds.		Pedogenically altered floodplain or shallow-water clay.
F10. Clay with vertic cracking.		Diatomaceous clays with siliciclastics and volcanic glass. Distinctive vertical mudcracks. Carbonates sometimes present.	Scarce freshwater diatoms (mainly <i>A. granulata</i>), sponge spicules, phytoliths common. Burrows and bioturbation.	Desiccated floodplain or lacustrine sediment, pedogenically altered.
F11. Granular clay.	Ct	Dark green clay, siliclastics, volcanic glass, minor pyrite. Granular texture with millimeter-scale rounded clay pellets. Carbonates sometimes present.	Scarce freshwater diatoms (mainly A. granulata, R. gibberula), sponge spicules, phytoliths common. Burrows and bioturbation. MnO dendrites sometimes present.	Pedogenically altered floodplain or lacustrine clay.
F12. Clay/silt (diatomaceous) with peds		Unlaminated and laminated sediments. Variable sediment composition, carbonates (c) sometimes present.		Pedogenically altered lacustrine or floodplain sediments.
F13. Silty and sandy gravels (pumiceous) gravels.	Gs(p)	Clast-supported, pumice and siliciclastics. Poor to moderate sorting, commonly rounded pumice (generally $< 3\ cm$).	Scarce often fragmented diatoms.	Pedogenically altered, fluvially transported pumice and ash.
F14. Silty sands and sandy silts.	Sz/Ss	Poorly to moderately sorted, weak to moderately laminated/bedded and massive siliciclastic silts and fine sands. Clay and volcanic glass present with scattered pumice locally.	Scarce planktonic (<i>A. agassizi</i> , <i>A. granulata</i>) and shallow water taxa (<i>H. amphioxys</i> , <i>R. gibberula</i> , <i>R. vermicularis</i> , <i>E. muelleri</i> , <i>C. placentula</i>). Sponge spicules/phytoliths; Botryococcus.	
F15. Zeolitic silty clays and clayey silts.	Czx/ Zcx		Diatoms generally absent. Scarce phytoliths, pollen. Algal (?) organic matter. Charcoal present.	Saline lake.
F16. Zeolitic silty sands.	Ssx	Analcimic silty sand interbedded with Facies 14. Associated with double clay laminae in a few sections. Volcanic glass abundant (up to 70%) with siliciclastics. Granule-size pumice scattered through the sediments and concentrated in horizons.		Shallow (?) saline lake.
		parmee seattered through the seaments and concentrated in nonzons.		(tidt)

,				
Primary Lithologies	Facies code	Primary Lithologies Facies Lithology, structure code	Associated features and diatom content	Environment
F17. Zeolitic gravell sands.	y Sgx	F17. Zeolitic gravelly Sgx Massive analcimic silty/gravelly sands interbedded with F14 and F15. Volcanic glass, Diatoms absent, charcoal present. sands. siliciclastics, pumice, lithic, and carbonate clasts, which tend increase in size towards base.	Diatoms absent, charcoal present.	Debris flow deposit into saline Early diagenetic zeolite (?)
F18. Zeolitic laminated silts.	Zlx	Hardened zeolitic laminated silts. Includes horizontal and ripple laminae, some slightly sandier. Volcanic glass generally dominates with common siliciclastics. Saline lake mineral assemblages common, including analcime, merlinoite, mordenite.	Diatoms absent, charcoal present.	Laminations and lack of diatom suggest saline lake. Zeolites eit! lacustrine or early diagenesis (
F19. Volcaniclastic silts/sands/gravels.		Zv/Sv/ Alternating clast-supported pumice gravel and dark sandy silts dominated by Diatoms absent. S Gv volcanic glass. Calcareous clay horizons, root traces, burrows. Cross-laminae and cut charcoal present. and fill structures.	Diatoms absent. Scarce phytoliths in finer-grained materials, charcoal present.	Shallow water to subaerial. Flu influence.
F20. Bedded gravels. Gb	s. Gb	Coarse-grained siliciclastics up to 5 mm. Massive/well bedded. Pyrite and volcanic Scarce shallow fresh to mildly saline, often fragmented, diatoms, glass present. Some fining-upward sequences and inclined bedding. Erosional scours. possibly reworked.	Scarce shallow fresh to mildly saline, often fragmented, diatoms, possibly reworked.	Fluvial (with reworked lake sediments).
F21. Matrix- supported volcaniclastics.	Vt	Matrix-supported rounded pumice. Matrix includes volcanic glass, clay, siliciclastics, pyrite, root channels.	Matrix includes volcanic glass, clay, siliciclastics, Rare A. granulata (possibly reworked), sponge spicules and phytoliths.	Debris flow into fluvial setting
F22. Friable, clayey Scf/ silts and gravelly Szf/ sands. Sgf	Scf/ Szf/ Sgf	Light brown/augured upper 27 m. Loose, moderately to poorly sorted volcaniclastic Variable pumice (<3 cm); rare shallow-water diatoms, plant debris. Fluvial and floodplain deposits, clays, silts, sands and gravels. Loose and massive.	Variable pumice (<3 cm); rare shallow-water diatoms, plant debri Reworked silt and diatomite clasts (<0.5 cm).	s. Fluvial and floodplain depos aeolian contributions?

Ę,

representative examples of each shown in Fig. 3. Simplified lithologic logs are presented in Figs. 4 and 5, together with representative sedimentological features in core photographs. The sediments are comprised of primary ash and pumice, reworked volcaniclastics, clay, siliciclastics and carbonate mud as well as biogenic siliceous (diatoms, sponge spicules, phytoliths) and organic (charcoal, amorphous algal debris, rare pollen and spores) components (Deino et al., 2019). Calcium carbonate is present as authigenic crystals in some diatomaceous muds, as micrite, pedogenic carbonate, and ostracods in a few beds. Calcite is most abundant above ~45 m and below 130 m. Quartz, feldspar, clay and volcanic glass are present, varying in proportion. XRD data indicate a range of zeolites dominated by analcime and phillipsite, with less frequent merlinoite, mordenite, natrolite and garronite.

The classification of diatomaceous sediments follows that of Owen (2002). Massive, bedded and laminated subdiatomite and diatomaceous silt and clay with well-preserved diatoms are present in many parts of the core with reworked diatom fragments sometimes present. Non-diatomaceous, zeolitic deposits are also present between ~63 and 107 m, often with clay laminae, locally in distinctive paired sets. Diatom sampling avoided well-developed burrows and termite chambers that postdate episodes of lacustrine sedimentation. Slumped units are rare. Pedogenic alteration is widespread and is associated with disrupted bedding, massive units, mudcracks, peds, root systems, burrows and carbonate nodules. Planar erosion surfaces and minor channelling are also present. Differing degrees of pedogenesis have variably altered preexisting diatomaceous sediments, contributing to partial mixing of diatom assemblages. However, while several strongly altered soils lack diatoms, others retain a clear diatom stratigraphy, especially those with evidence of bedding. In these cases, sharp boundaries between assemblages in different horizons indicate that valve translocation is limited.

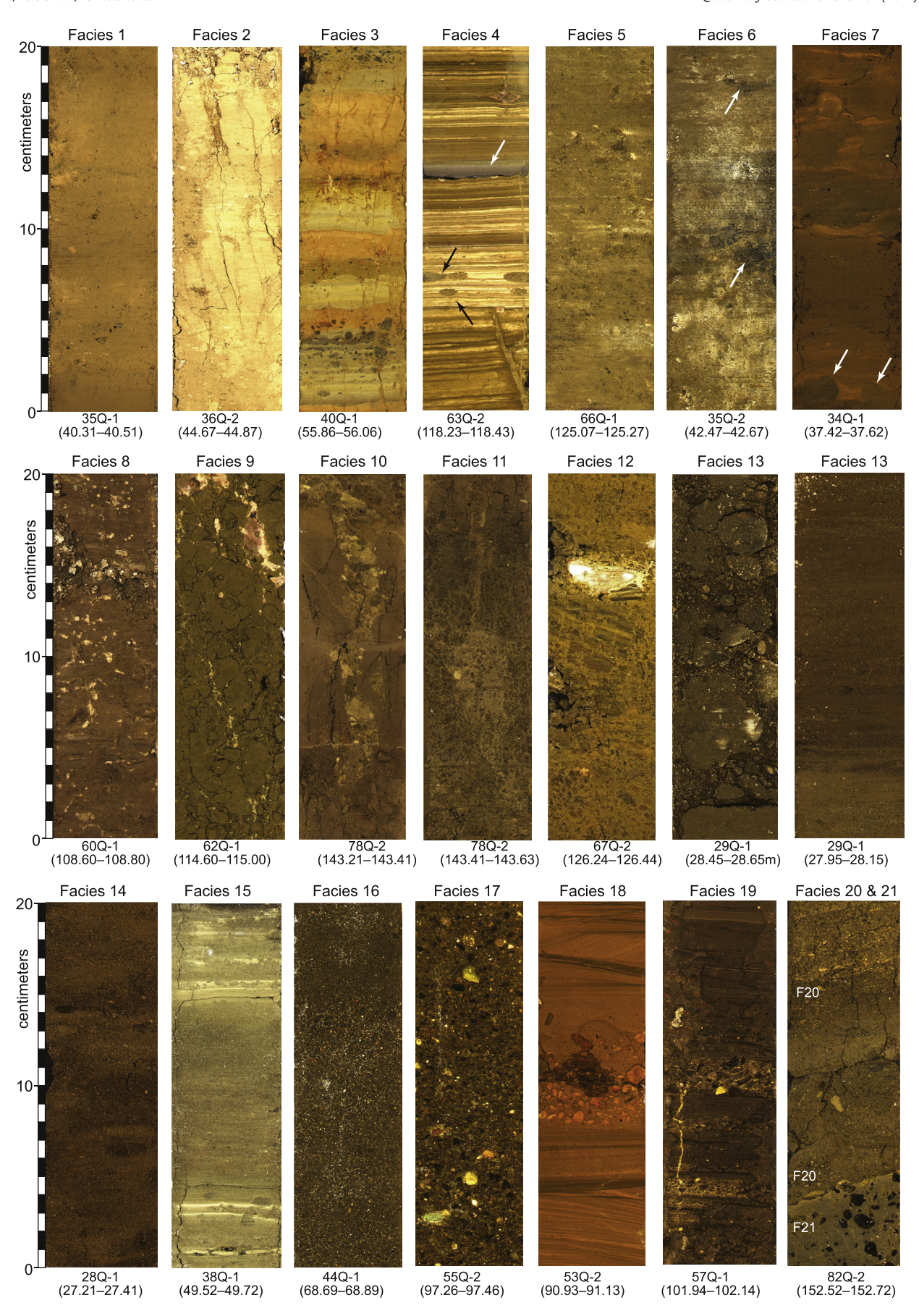
4.2. Diatom stratigraphy

The Koora deposits include 105 diatom taxa in 600 samples (Table S1). Diatoms associated with differing facies are noted in Table 1. Freshwater Aulacoseira spp. comprise >75 % of the assemblages in subdiatomite (Facies F1 to F3) with saline taxa associated with F2 and silty units in F3. Laminated diatomite and clay (F4) contain at least 75 % A. granulata and A. agassizii with no saline planktonic species. Diatomaceous clay and silt facies (F5-F7) contain more varied benthic taxa. Pedogenically altered deposits (F8-F11) contain a variety of planktonic and benthic species reflecting pre-existing lacustrine and fluvial settings. Diatoms are scarce in reworked lake and floodplain deposits (F12-F14), and consist mainly of benthic taxa. Highly saline palaeolakes characterised by zeolites (F15–F18) lack diatoms, which probably did not grow during deposition, although post-depositional dissolution is also possible. Diatoms are absent in fluvial and debris flow units (F19–F22), other than as reworked fragments.

Visual identification of 41 zones was based on the presence or absence of diatoms, the proportions of benthic versus planktonic taxa and the percentage of saline diatoms (mainly *Thalassiosira* spp., *Cyclotella meneghiniana*) with each zone representing an average of ~24,400 years. The diatom stratigraphy is shown in Figs. 4 and 5, which groups the zones into five major stratigraphic units using criteria outlined below. Individual taxa referred to as 'dominant' comprise >25 % of an assemblage. Diatom assemblages are described as rare (<10 3 valves g $^{-1}$), sparse (10 3 –10 7 g $^{-1}$), common (1–6 x 10 7 g $^{-1}$) and abundant (>6 × 10 7 valves g $^{-1}$).

4.2.1. Unit I (161.80–134.5 m; ~1006.8–460.5 ka)

Unit 1 is characterised by coarse-grained facies (F19-22) that



give way upwards to diatomaceous silt and subdiatomite (F1–5). The unit mostly contains 20–100% freshwater *Aulacoseira* spp. (Fig. 4) with sponge spicules and phytoliths present throughout. Diatom valves are common in Zone 1 (161.81–157.3 m), with *Aulacoseira agassizii* dominating and *Aulacoseira granulata*, *Encyonema muelleri*, *Cocconeis placentula* and *Epithemia* spp. also present. Zone 2 (157.30–149.48 m) diatoms are often fragmented and generally scarce or absent. *Aulacoseira granulata* dominates except near the base, which variably contains *A. agassizii*, *C. placentula* or *Rhopalodia vermicularis*. *Nitzschia palea* and *A. agassizii* increase close to the top of the zone.

Zones 3 (149.48–136.50 m) and 5 (134.9–134.5 m) contain common to abundant diatoms, dominated by *A. granulata* with Zone 4 lacking valves. Floral variations mainly reflect changing percentages of *A. agassizii*, *A. ambigua*, *A. granulata* var. *valida*, *A. granulata* var. *angustissima*, *Cyclotella meneghiniana* and rare *Thalassiosira rudolfi*. *Encyonema muelleri*, *C. placentula* and *R. vermicularis* dominate the scarce benthonic flora.

4.2.2. Unit II (134.5–107.07 m; ~460.5–254.5 ka)

Unit II is comprised of diatomaceous silt, subdiatomite and laminated diatomite and clay (Facies 1–7). Pedogenic alteration is present (Facies 8–11) as are examples of burrowed lake sediments (Fig. 4C,E). The assemblages are distinguished by the co-occurrence of saline and freshwater taxa with greater assemblage variability than Unit I. Zone 6 (134.50–131.90 m) contains abundant diatoms and low percentages of Aulacoseira with saline (*T. rudolfi, Anomoeoneis sphaerophora, Craticula elkab*) and euryhaline (*C. meneghiniana*) species increasing. Discostella pseudostelligera, Mastogloia braunii, Epithemia adnata, Nitzschia spp. and Rhopalodia gibberula are also regularly present (Fig. 4).

Zone 7 (131.90–131.32 m) is dominated by *Hantzschia amphioxys* and *T. faurii* in some samples. Zone 8 (131.32–130.02 m) is dominated by *D. pseudostelligera* and minor saline and benthonic taxa. Zone 9 (130.02–122.52 m) includes both freshwater and saline diatoms. Valves are common with *A. agassizii* dominating and *T. faurii* and *A. sphaerophora* consistently present. *Cyclotella meneghiniana*, *A. granulata* var. *angustissima*, *E. muelleri*, *Rhopalodia* spp. and *Epithemia* spp. are also present, with an increase in both benthonic and epiphytic diversity compared with zones 7 and 8.

Zone 10 (122.52—118.78 m) is characterised by common diatoms with high percentages of *A. agassizii* with *A. granulata, E. muelleri, Epithemia sorex, A. sphaerophora, R. gibberula* and *H. amphioxys* variably present. Frustule abundances increase in Zone 11 (118.78—118.20 m) with *A. granulata, A. granulata* var. *angustissima* and *T. faurii* each ranging between 5 and 75% of the assemblages. Zone 12 (118.20—116.37 m) contains common to abundant valves comprised of >80 % *Aulacoseira* (*A. granulata, A. granulata* var. *angustissima, A. agassizii, A. agassizii* var. *malayensis*) and less frequent *C. placentula, E. muelleri, C. meneghiniana, Pantocsekiella ocellata, R. vermicularis* and *Ulnaria ulna*.

Diatoms are common to abundant in Zone 13 (116.37–113.20 m) with *A. agassizii* and var. *malayensis* dominant through most of the zone and with less frequent *A. granulata*, *C. placentula*, *Diploneis ovalis*, *A. sphaerophora*, *R. gibberula*, *R. vermicularis* and *H. amphioxys*. Zone 14 (113.20–110.09 m) includes *T. faurii* and *T. rudolfi* together with *Rhopalodia* spp., *Epithemia* spp.,

A. sphaerophora, C. elkab, M. braunii, C. placentula and Nitzschia spp. with intermittently present Discostella stelligera, D. pseudostelligera, A. granulata and A. agassizi.

Zones 15–16 contain fewer diatoms. *Cocconeis placentula* and *Epithemia* taxa dominate in Zone 15 (110.09–108.96) with *Nitzschia* spp. and *Rhopalodia* spp. also present. *Hantzschia amphioxys* dominates in Zone 16 (108.96–107.07 m) with *A. agassizii* and var. *malayensis* and *R. gibberula* also present.

4.2.3. Unit III (107.07-66.05 m; ~254.5-212.2 ka)

Diatoms are absent from large parts of the zeolitic sediments (Facies 15–18) of Unit III. Where present, dissolution is minimal, including Zone 17 (107.07–101.80; Fig. 4) where *D. pseudostelligera* and *E. argus* dominate sparse assemblages in two separate samples. They are rare or absent in Zone 18 (101.80–100.90 m, Fig. 5), where *A. granulata* var. *valida*, *C. meneghiniana* and *C. placentula* dominate. Zone 19 (100.90–100.60 m) is dominated by either *C. meneghiniana* or *D. pseudostelligera* with less frequent *D. stelligera*, *A. sphaerophora* and *R. gibberula*. Zone 20 (100.60–97.73 m) includes common to abundant diatoms with the most frequent taxa including *A. agassizii*, *C. meneghiniana*, *A. sphaerophora*, *R. gibberula*, *Epithemia argus*, *C. placentula*, *Rhopalodia gibba*, *Nitzschia* spp. and *Surirella ovalis*, which is absent in both zones 19 and 21.

Zones 21 (97.50–81.46 m), 23 (80.50–76.68 m) and 26 (74.21–66.05 m) lack diatoms. Zone 22 (81.46–80.50 m) contains frequent *E. argus* (10–79 %) and *C. placentula* (10–25 %). Zones 24 (76.68–75.74 m) and 25 (75.74–74.21 m) also contain sparse to common diatoms with *E. argus* dominant at many levels. Zone 24 includes variable percentages of *A. agassizii*, *C. meneghiniana*, *T. faurii*, *D. ovalis*, *H. amphioxys* and *Nitzschia lancettula*, which are absent or rare in Zone 25, where *R. gibberula* or *H. amphioxys* intermittently form >20 % of the assemblage.

4.2.4. Units IV (66.05–27.00 m; ~212.2–83.5 ka) and V (27.00–0 m; ~83.5–0 ka)

The sediments of Unit IV include clay, diatomaceous silt, subdiatomite, sand and palaeosols. Zeolites and less frequent dolomite and Mg-calcite are present in many horizons. Diatom assemblages are variable with zones dominated by freshwater or saline or mixed salinity taxa (Fig. 5). Zone 27 (66.05–64.78 m) contains sparse to common diatoms dominated by *C. meneghiniana* with *R. gibberula* comprising >15 % of the assemblages. Caution is required with interpretation of diatoms in Zone 28 (64.78–58.57 m) where diatoms are sparse to absent and *C. meneghiniana* and *E. argus* are generally dominant with less frequent *Aulacoseira* species. *Rhopalodia gibba* is dominant in one horizon with very low abundance. Diatoms are common in Zone 29 (58.57–56.26 m) where *E. argus* and *A. agassizii* dominate and *R. gibberula* percentages increase.

Diatoms are abundant in Zone 30 (56.26–55.24 m), where *A. agassizi* and *A. ambigua* form the highest percentages with less frequent *P. ocellata* and *E. sorex*. Zone 31 (55.24–53.75 m) taxa are characterised by common diatoms with frequent saline species, including *C. meneghiniana*, *C. elkab* and *A. sphaerophora*. Diatoms are absent to common in parts of Zone 32 (53.75–47.99 m) where benthic taxa (*E. argus*, *E. adnata*, *R. gibberula*, *Rhopalodia hirundiformis*, *Nitzschia frustulum*, *N. palea*) increase in percentage terms.

Fig. 3. Facies types in Core ODP-OLO12-1A. See Table 1 for descriptions. Core segment number and depth below surface (m) below each photograph. F1: Massive diatomite/subdiatomite. F2: Massive calcareous diatomite/subdiatomite. F3: Bedded diatomite and clayey/silty diatomite. F4: Laminated diatomite and clay. White arrow indicates ash, black arrows point to burrows. F5: Diatomaceous clayey silt with vague bedding. F6: Diatomaceous organic-rich silt. Arrows point to diffuse organic-rich patches. F7: Silty clay with clay laminae. Arrows point to laminae draping over pumice. F8: Silts with carbonate nodules. F9: Clay with peds. F10: Clay with vertic cracking. F11: pelleted clay. F12: Brecciated clay/silt. F13: Silty and sandy gravels. Two images, 29Q-1 fragmented. F14: Silty sands and sandy silts. F15: Zeolitic silty clays and clayey silts with laminae, often paired. F16: Zeolitic silty sands. F17: Zeolitic gravelly sands. F18: Zeolitics diaminated silts, with ripples and pumice bed. F19: Volcaniclastic silts/sands/gravels with interbedded pumice, silty and sandy units. F20 and F21: Bedded gravels. (F20) resting on eroded surface into matrix-supported volcaniclastics (F21).

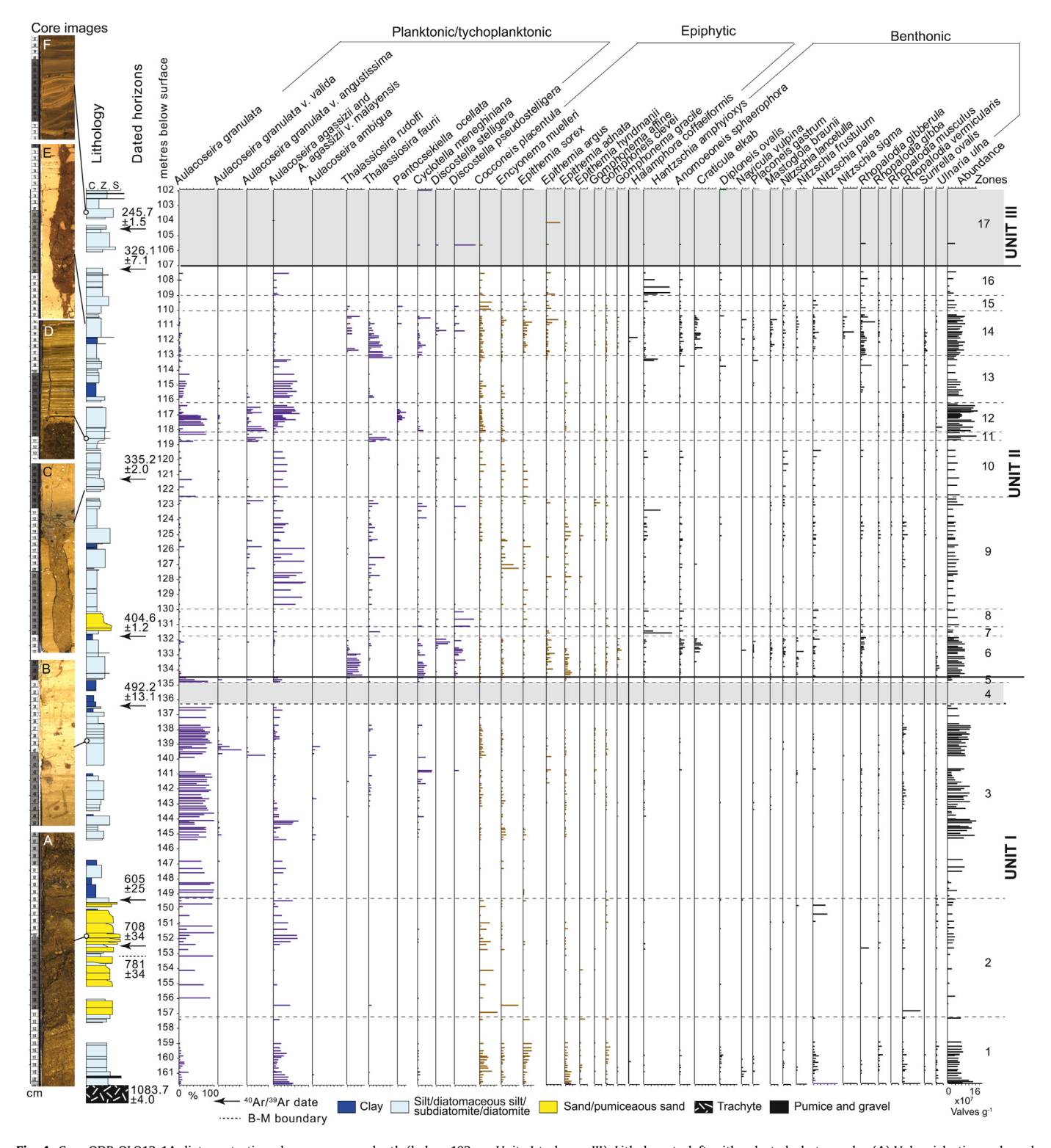


Fig. 4. Core ODP-OLO12-1A diatom stratigraphy versus core depth (below 102 m; Units I to lower III). Lithology to left with selected photographs. (A) Volcaniclastic sands and gravels and bedded gravels, (B) Faintly bedded subdiatomite, (C) Burrow in subdiatomite, (D) Laminated diatomite and clay, (E) Termite burrow in massive diatomite, (F) Zeolitic silty clay. Diatom stratigraphy and zones to the right include only common diatoms (>10 % in at least one sample). Grey shading indicates intervals where diatoms are absent. See text for discussion.

Zones 33 (47.99–47.83) and 34 (47.83–45.48 m) contain sparse to common diatoms. The former zone is dominated by *A. agassizii*, which gives way to *H. amphioxys* in Zone 34 where *R. gibberula*, *C. meneghiniana*. *P. ocellata* and *A. granulata* are also intermittently dominant. *Caloneis bacillum* is relatively frequent (5–36%) in zones

33 to 35 compared with other parts of the core. Zone 35 (45.48–42.50 m) contains common to abundant valves generally dominated by *T. faurii*, with *T. rudolfi* and *C. meneghiniana* also intermittently dominant. The zone is also characterised by high apparent diversity, compared to both Zones 34 and 36, with the

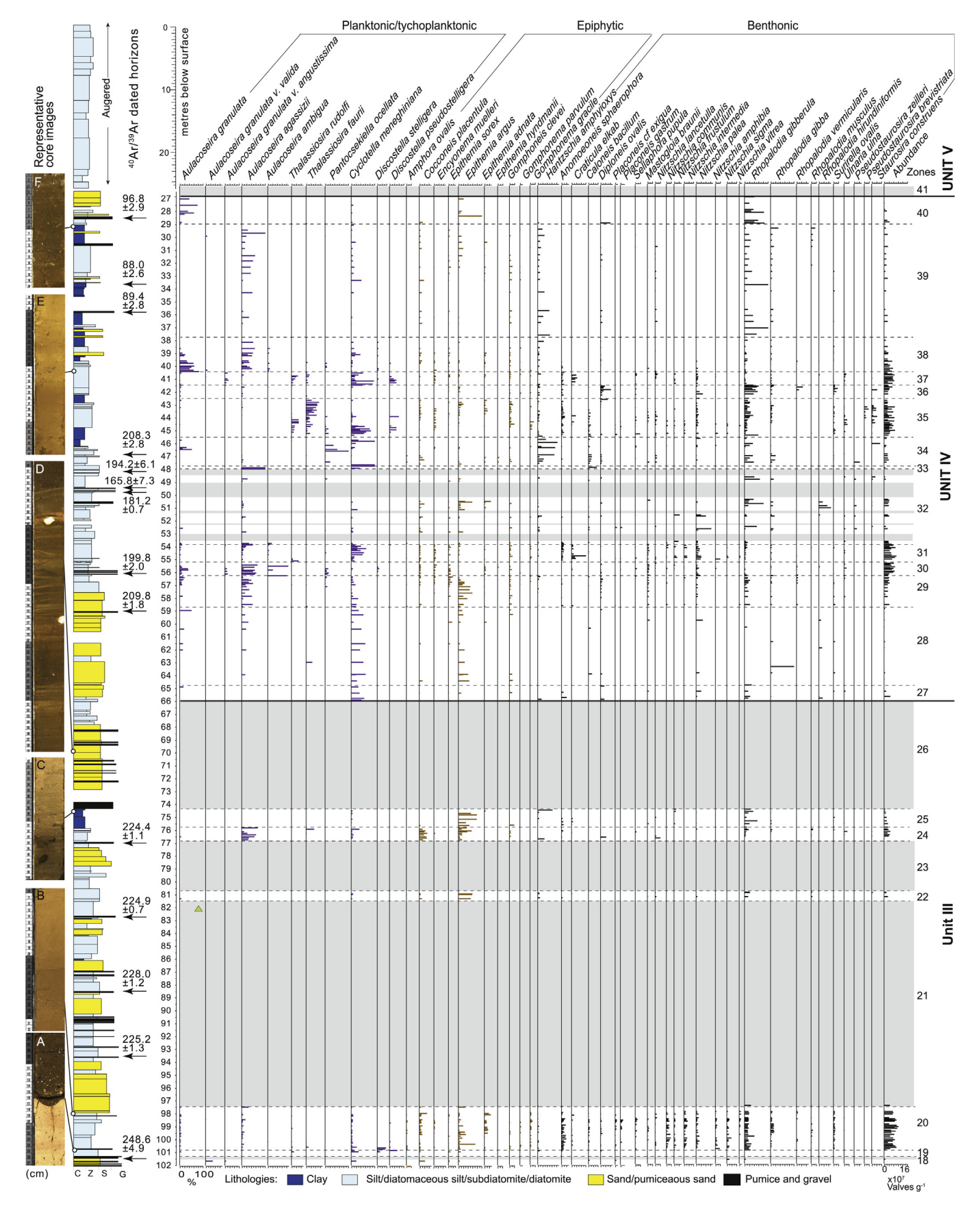


Fig. 5. Core ODP-OLO12-1A diatom stratigraphy *versus* core depth (above 102 m; Units III to V). Lithology shown to left with selected photographs. (A) small channel cut into diatomite, (B) Massive subdiatomite, (C) Diatomaceous clay, (D) Zeolitic silty clay, (E) Massive subdiatomite, (F) Diatomaceous silty clay. Diatom stratigraphy and zones to the right include only common diatoms (>10 % in at least one sample). Grey shading indicates intervals where diatoms are absent. See text for discussion.

almost constant presence of all taxa represented in the diatom diagram, except *Aulacoseira* species. Zones 36 (42.50–41.48 m) and 37 (41.48–40.40 m) contain sparse to common valves. Zone 36 is dominated by *R. gibberula* with benthic taxa and diatoms often associated with very shallow swamps (*D. ovalis*, *H. amphioxis*) also present. Zone 37 is characterised by *C. meneghiniana* (20–95%) with less frequent *T. rudolfi*, *T. faurii*, *C. elkab* and *D. pseudostelligera*. Zone 38 (40.40–37.73 m) is dominated by either *Aulacoseira agassizii* or *A. granulata* with the latter decreasing and finally disappearing towards the top of the zone.

Diatoms are variously absent, sparse or common in Zone 39 (37.73–28.98 m), where they are dominated by *R. gibberula*, *H. amphioxys*, *C. meneghiniana* or *Aulacoseira agassizii* with the latter increasing upwards. Zone 40 (28.98–27.00 m) contains sparse diatoms with *R. gibberula*, *A. granulata* and *E. argus* intermittently dominating. Diatoms are absent through most of the overlying sediments of Zone 41 (= Unit V), which are composed of loose augered silts, although rare *R. gibberula* were observed in several samples.

5. Discussion

5.1. Diatom ecological preferences

Fig. 6A shows a correspondence analysis (CA) for 65 taxa. Axis 1, which explains 66.6% of the variance, is related to water depth, suggested by a high correlation with the sum of the percentages of planktonic *Aulacoseira* and *Stephanodiscus* (r = -0.959, p < 0.001). Planktonic diatoms are associated with positive axis 1 values with benthic taxa showing negative values. The axis data forms an important part of subsequent interpretations (Fig. 7). In contrast, Axis 2 (24.7% variance) reflects diatom salinity preferences, with saline species displaying negative values. *Discostella pseudostelligera*, *Nitzschia amphibia* and *Nitzschia recta* are commonly cited as freshwater taxa, but overlap with the field of saline diatoms in Fig. 6A. The latter diatom is relatively scarce among the assemblages with the two others, *D. pseudostelligera* and *N. amphibia*, also reported as salt tolerant (Gasse, 1986).

An Agglomerative Hierarchical Clustering (AHC) for 38 diatoms documents ten clusters at 0.5 dissimilarity (Fig. 6B), reflecting diatom ecological preferences. The latter are the basis for habitat interpretations shown in Fig. 7. Diatom groups I-IV include subaerial to shallow-water taxa associated with fresh to moderately saline water. Group I comprises D. ovalis and Hantzschia amphioxys, which are aerophilic and found in freshwater swamps and damp soils (Owen et al., 2004, 2008b, 2008b). Group II includes salt tolerant, littoral benthic A. sphaerophora, R. gibberula, Nitzschia communis and Nitzschia sigma, which are present in waters of variable salinity and alkalinity (Gasse et al., 1995; Legesse et al., 2002). The littoral freshwater to mesohalobous Surirella ovalis also belongs to Group II (Gasse, 1986). In contrast, Group III taxa (R. gibba, Gomphonema gracile and E. adnata) are predominantly oligohalobous, benthic and epiphytic, indicating shallow freshwater habitats with abundant macrophytes. Group IV (N. amphibia, Sellaphora pupula and C. bacillum) is dominated by fresh littoral taxa, often associated with springs (Lee et al., 2013). Owen et al. (2004) recorded these diatoms in wetlands and springs near Lake Bogoria with pH values of 7.2, 6.8 and 7.3, respectively. Gasse (1986) described them as freshwater littoral, crenophile taxa associated with slightly higher pH values of 7.67-8.44.

Groups V–VII are characterised by moderately to highly saline species. Group V includes brackish water, littoral *Mastogloia braunii* and *E. argus* (Gasse, 1986) together with *D. stelligera*, which is present in both planktonic and littoral settings in small dilute to mesohaline lakes (Gasse, 1986; Owen et al., 2008a). Group VI

includes only planktonic *Thalassiosira faurii* with a conductivity optimum of ~9000 μ S.cm $^{-1}$ (Gasse et al., 1995; Telford and Lamb, 1999). Roubeix et al. (2014) suggested a much lower optimum of 400 μ S.cm $^{-1}$, but this taxon is mostly found with other highly saline taxa. Group VII diatoms typically display negative values on CA axes 1 and 2, suggesting moderate to high salinity. *Cyclotella meneghiniana* is a facultative planktonic taxon associated with alkalinities of ~4–50 meq l $^{-1}$ (Richardson et al., 1978; Zalat and Servant-Vildary, 2007) and an optimum pH of ~8.85 (Gasse et al., 1995). *Craticula elkab* is associated with *Nitzschia frustulum*, both reported from shallow saline settings and hot springs (Owen et al., 2004, 2008b).

Groups VIII to X are representative of freshwater lakes. Group VIII includes planktonic *Aulacoseira*. *Aulacoseira* granulata is common in freshwater lakes (conductivities = $47-1300 \mu S.cm^{-1}$; pH = 6.5-9; Gasse, 1986, 1987) and is favoured by relatively high silica (>10 mg l⁻¹; Kilham and Kilham, 1975), outcompeting *A. ambigua* and *A. agassizii* as phosphorus increases and light levels decrease. *Aulacoseira* agassizii and variety malayensis are present in shallow dilute water ($<500-1100 \mu S.cm^{-1}$; pH 8-8.5; Richardson and Richardson, 1968; Gasse, 1986). Planktonic *A. ambigua* is favoured by fresh shallow water ($<7 \text{ meq l}^{-1}$; pH 6.5-8) on the margins of larger lakes (Richardson et al., 1978). Gasse et al. (1995), suggest a pH optimum of \sim 8.5 for *P. ocellata*. All Group VIII taxa were common in the Olorgesailie palaeolakes to the north (Owen et al., 2008a).

Group IX includes littoral, epiphytic, freshwater *Gomphoneis clevei* and *Ulnaria ulna* with pH optima of 6.43 and 7.71, respectively (Gasse et al., 1995). The latter taxon is capable of entering the plankton, but its association with *G. clevei* suggests a shallow setting (Gasse, 1986). Group X is dominated by freshwater to slightly brackish, littoral and epiphytic diatoms such as *Amphora ovalis*, *E. sorex* and *E. muelleri*, which are found in lakes with a pH > 8, together with epiphytic *C. placentula* (pH 7.5–8). Limnobiontic *R. vermicularis* is also present but is found in a variety of fresh to hyperalkaline waters (Gasse, 1986).

5.2. Environmental stratigraphy

Fig. 7 shows diatom-based habitat, conductivity and pH data plotted against the Koora age model (Deino et al., 2019). CA Axis 1 is also plotted and serves as a proxy for relative water depth, reflecting benthic vs. planktonic taxa, with positive values indicating deeper water. Diatom diversity is reflected in the Simpson 1-D index, with the highest values associated with shallow lake phases, especially during Zones 2, 6, 14 and 20.

Aquatic deposition was interrupted by desiccation and soil formation 30 times with increased frequency after 400 ka, or by minor erosion events (Fig. 7) (Potts et al., 2020). Termite and other non-aquatic burrowing organisms penetrated through lake sediments (Fig. 4C,E) with non-deposition surfaces also indicating termination of lacustrine episodes (Fig. 5A). Diatoms are absent in several segments of the core. This is partly explained by terrestrial deposition, but other processes such as dilution by volcaniclastics, fragmentation and winnowing, or dissolution could also explain an absence of diatoms. The presence of zeolitic laminated sediments with no diatoms suggests lake and/or pore waters were highly alkaline, which may have caused post-mortem dissolution. However, the absence of diatoms may also reflect their absence in these palaeolakes.

5.2.1. Unit 1 (~1006.8-460 ka; 161.8-134.5 m)

The lacustrine sediments in this unit were laid down in deep to shallow freshwater lakes that periodically dried out (Fig. 7). It is also important to note that this part of the core is temporally less

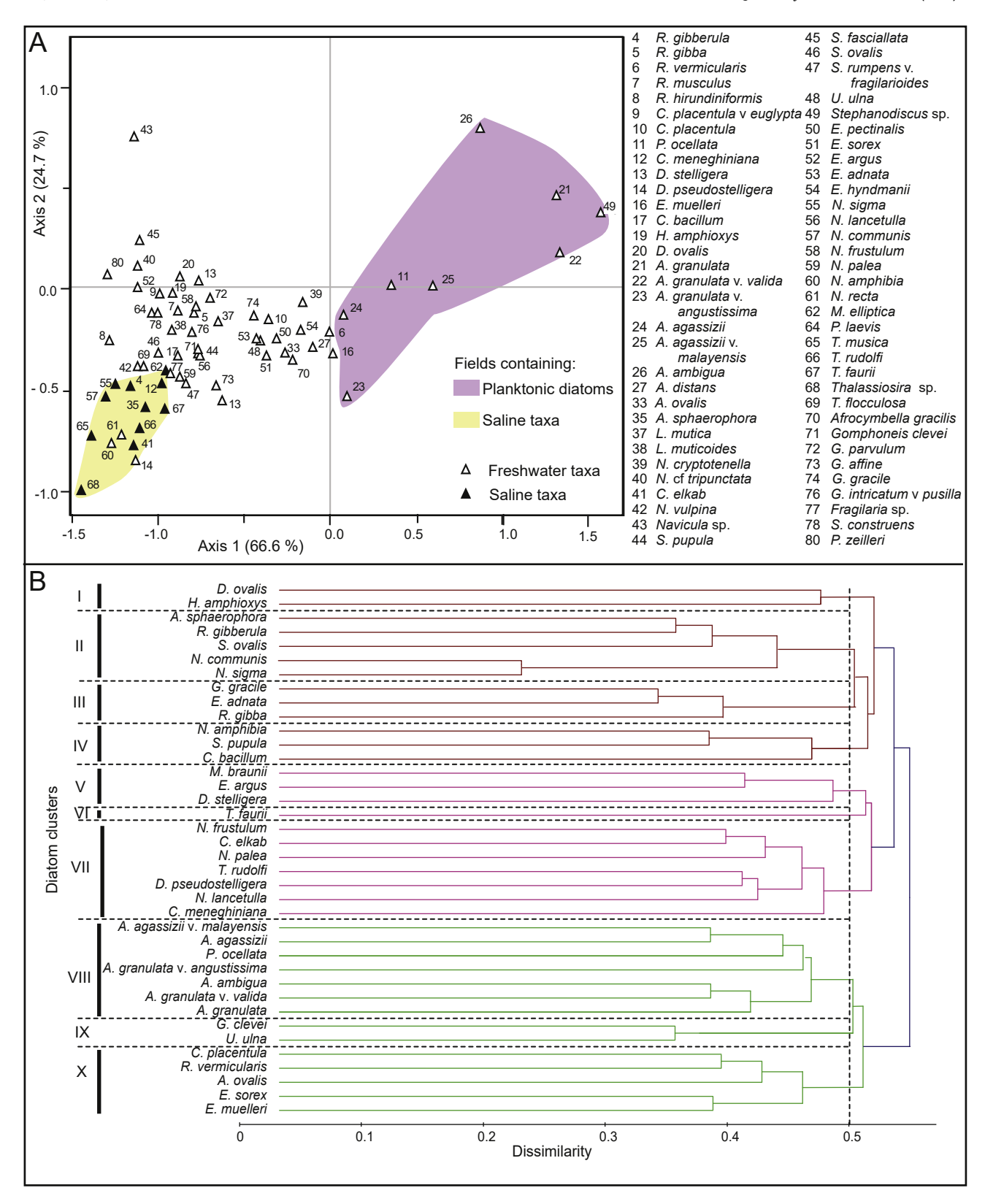


Fig. 6. Statistical representations of diatom assemblages. A) Correspondence Analysis. Freshwater planktonic and benthic forms separated along Axis 1. Axis 2 reflects salinity with highly saline taxa concentrated in the lower left and characterised by negative values. B) Agglomerative Hierarchical Clustering of diatoms showing ten diatom groups at 0.5 dissimilarity.

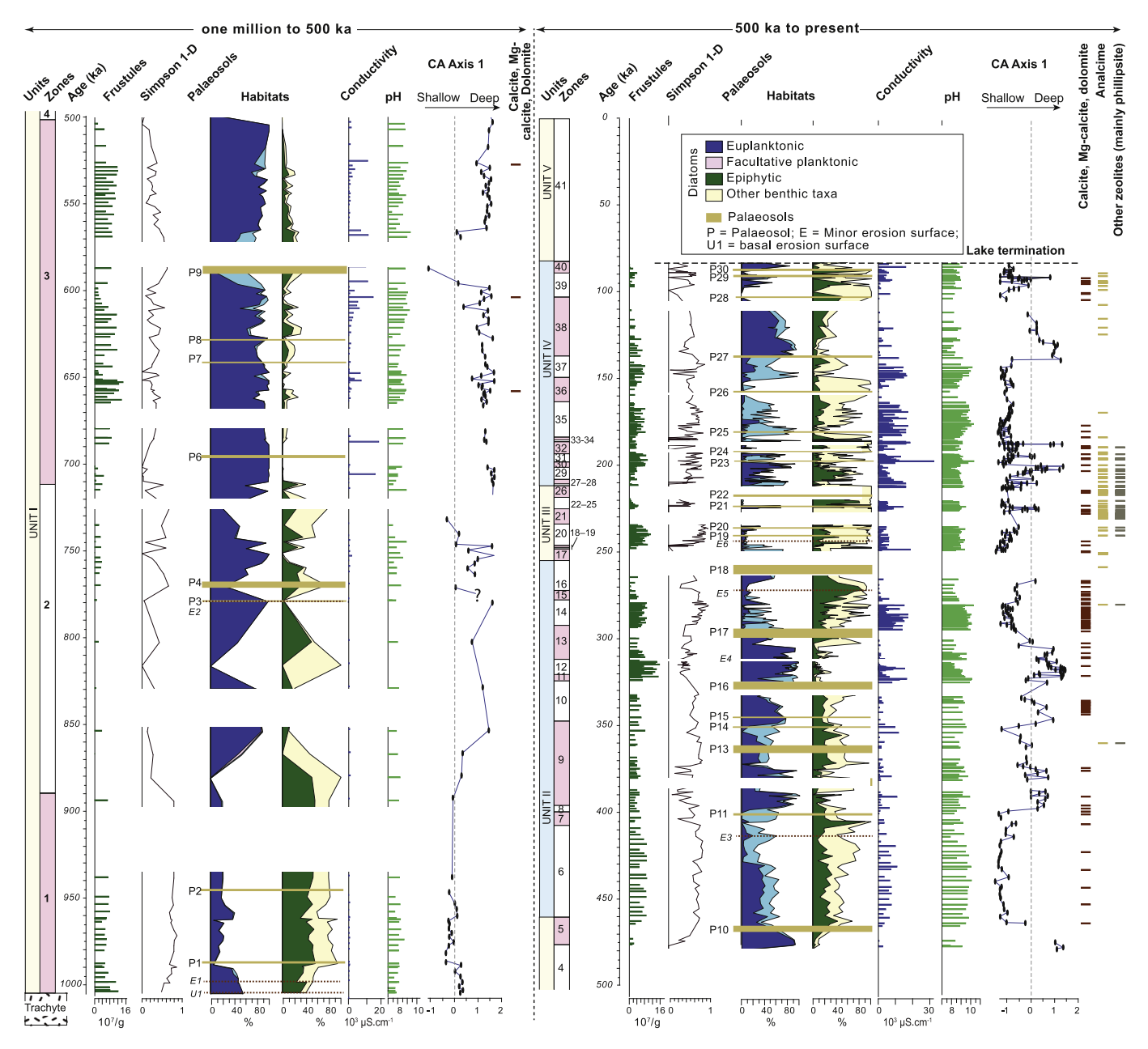


Fig. 7. Environmental reconstructions. Diatom-based aquatic habitats, conductivity and pH (ODP-OLO12-1A) plotted against time (1–0.5 Ma and 0.5–0 Ma; based on age model of Deino et al., 2019). Zones can be used to compare against diatom assemblages in Figs. 4 and 5. Note numerous palaeosols (labelled P) indicate periods when lakes dried out (after Potts et al., 2020). Positive CA Axis 1 scores reflect deeper water. Authigenic minerals to right. Carbonates suggest slightly higher salinities with analcime and zeolites indicating very saline lakes and/or pore water.

well sampled and may underestimate environmental/climate variability than the better-resolved younger sediments above. Zone 1 (~1007–891 ka; 161.81–157.3 m) is associated with diatomaceous silt and subdiatomite (Facies 1 and 5; Table 1). The diatoms (Assemblages I and II, Fig. 6B) are typical of shallow dilute water. *Aulacoseira agassizii* are present together with epiphytic species (Figs. 5 and 7), indicating intermediate water depths and/or nearby shallow habitats with aquatic macrophytes. Transfer functions suggest conductivities of $300-1000~\mu S.cm^{-1}$ and pH values of 8-8.8. Occasional lake desiccation is indicated by pedogenesis and minor erosion surfaces (Fig. 7).

Zone 2 (~891–713 ka; 157.30–149.48 m) is characterised by fresh to mildly alkaline benthic and epiphytic taxa, in low to moderate numbers, together with *A. granulata* (Assemblage VIII,

Fig. 6B), which indicates a series of shallow to moderately deep waters (Fig. 7). Transfer functions indicate $250-900~\mu S.cm^{-1}$ with a pH of 8–9. Diatoms are partially fragmented, reflecting some reworking. In contrast, fluvial and terrestrial conditions are indicated by the presence of pedogenic alteration, minor erosion surfaces and coarse-grained quartzo-feldspathic facies (F19–F21, Table 1; Fig. 4A), several of which fine upwards. The zone shows at least three cycles from shallow to deeper lake and back again, with the P4 palaeosol capping a regression. The erosion surface (E2) is developed immediately above a euplanktonic cycle and is followed by benthic assemblages, suggesting a shallowing event.

Zones 3 (~713–503 ka; 149.48–136.50 m) and 5 (~476–460 ka; 134.9–134.5 m) include a variety of diatomaceous facies characterised by an increase in planktonic taxa, mainly *A. granulata*,

reflecting deeper water than Zones 1 and 2 (Fig. 7). Nevertheless, conditions did vary with palaeosols indicating emergence. Parts of Zone 3 also include *Thalassiosira* suggesting intervals with higher conductivities (up to 19,000 µS.cm⁻¹) although most of this zone is characterised by values < 5000 µS.cm⁻¹. Furthermore, a lack of diatoms in Zone 4 coincides with a modified clay that may have been disturbed by drilling mud.

5.2.2. Unit II (~460.5-254.5 ka; 134.5-107.07 m)

Unit II sediments were laid down in hypersaline to fresh and shallow to deep lakes, which periodically dried out (Fig. 7). CA Axis 1 suggests that shallow palaeolakes dominated during most of Unit II times, but with several deeper lake phases. Deeper lakes led to accumulation of massive, bedded and laminated subdiatomite and diatomite (F1–F4, Table 1; Fig. 4B–E). However, these lacustrine sediments were repeatedly exposed and subjected to pedogenic alteration giving rise to a series of palaeosols (P11–P18). The top of one prominent soil horizon (P16, Fig. 7), for example, is overlain by finely laminated diatomite and diatomaceous clay (Zone 11, Fig. 4D) reflecting either a rapid change from a land surface to a deep freshwater lake or reduced sediment input to the depocenter, with increasing sediment storage up-dip during transgression. Higher in the sequence, Zone 14 also includes diatomite that was subsequently burrowed by termites after desiccation (Fig. 4E).

Increased salinities are implied by the presence of authigenic carbonates (calcite, Mg-calcite, dolomite) in the sediments. Very saline palaeolakes are indicated by diatom assemblages VI and VII (Fig. 6B) in parts of Zones 6, 9, 11, 12 and 14, with diatom-inferred conductivities that exceeded ~10,000 μ S.cm⁻¹. Benthic species are also present in all of these zones, with common freshwater planktonic diatoms (Assemblage VIII, mainly *A. granulata* and *A. agassizii*) mixed with saline species in Zones 9 and 11. The coexistence of saline and freshwater diatoms suggests either: 1) fresh deep waters that become seasonally or periodically more saline and perhaps shallower, followed by mixing of the different taxa in the sediments, or 2) the development of seasonal or periodic stratification with fresh water lenses overlying saline bottom water (Barker et al., 1990; Muiruri et al., 2021).

Salinity was generally reduced during formation of Zones 7, 8, 10, 13, 15 and 16, with inferred conductivities <8000 μS.cm⁻¹ and pH values of about 8.1–10. Freshwater lakes (~200–2200 μS.cm⁻¹) were also present during Unit II times and were variously dominated by *A. granulata* (Zone 5), *D. pseudostelligera* (Zone 8) and *A. agassizii* (Zone 10) (Fig. 4). Relatively shallow wetlands and swamps developed during the termination of Zone 13 and through Zone 16, which contain common *H. amphioxys* and *A. agassizii*. The uppermost sediments of Unit II include shallow water diatoms (Zones 15 and 16) with an increase in planktonic *Aulacoseira* toward the top of Zone 16 that suggests a deepening phase prior to regression and the development of a palaeosol (P18, Fig. 7).

5.2.3. Unit III (~254.5-212.2 ka; 107.07-66.05 m)

Unit III includes 41 m of sediment with diatoms present in only about 14 m (Figs. 4 and 5). In temporal terms, diatoms were accumulating through about 20 of the 43 kyr spanned by these deposits. This interval was characterised by increased inputs of tephra and deposition rates (Deino et al., 2019). Unit III was laid down in a series of saline to hypersaline lakes given the presence of carbonates and especially zeolites (analcime, phillipsite, mordenite and natrolite), which are common in the laminated and massive silt and clay (Figs. 5D and 7). Carbonates likely formed in the water column following evaporative concentration or microbial blooms that changed pH conditions (Kelts and Hsü, 1978). Zeolites reflect the alteration of volcaniclastic glass in saline, alkaline lake or pore water either at the time of deposition or during early diagenesis

(Surdam and Eugster, 1976; Owen et al., 2019), which, in turn, implies high evaporation rates and basin closure. The highly regular lamination in many parts of these deposits (Fig. 5D) indicates sufficient water depth to prevent wave-induced erosion and perhaps bottom water-anoxia (i.e. stratified lake) to prevent bioturbation from aquatic organisms. Palaeosols (P19—P22) and a minor erosion surface (E6) also suggest intermittent exposure.

The diatomaceous deposits include massive to faintly bedded calcareous silt and subdiatomite (F2, Table 1; Fig. 5A–C). Zones 18–20, 22, 24 and 25 all include common benthic taxa suggesting shallow lakes (Fig. 7). Shallow water, saline taxa (Assemblages II and VII, Fig. 6B) are common with *C. meneghiniana*, *A. sphaerophora* or *R. gibberula* variously dominant. Very shallow conditions are suggested by the presence of *H. amphioxys* in Zone 25. These diatomaceous zones formed in lakes with extremely variable conductivities ranging from 200 to 22,000 µS.cm⁻¹ and with pH values of 7.6–10.1. The coexistence of both freshwater benthic taxa and saline species might reflect seasonal or occasional flooding of an otherwise shallow saline lake. In contrast, Zone 24 contains common freshwater, planktonic and benthonic diatoms (e.g., *A. agassizii* and *C. placentula*), which indicate a short-term freshening and deepening of the Unit III palaeolakes.

Holocene Lake Nakuru in the central Kenya Rift may provide a somewhat similar example of extreme environmental variability over millennial time scales. Today, Lake Nakuru is shallow with conductivities of 23,100 to 96,200 μ S.cm⁻¹ (Jirsa et al., 2013). In contrast, during the early Holocene it was much expanded due to moister climates and was at least 100 times less concentrated than today (Richardson and Dussinger, 1986).

5.2.4. Unit IV (~212 ka-83.5 ka; 66.05-27.00 m)

Unit IV is characterised by a return to variable saline and freshwater lakes. Mg calcite and dolomite are intermittently present with analcime and/or phillipsite common in Zones 27-32 and analcime in Zones 33–39, indicating episodes of elevated salinities (Fig. 7). Diatom abundance fluctuates considerably being highest in Zones 29–31, 35 and 37 with the diatoms including abundant benthic and epiphytic species that are associated with freshwater and saline settings. Cyclotella meneghiniana, R. gibberula and H. amphioxys are more common than in Units I-III suggesting high salinities associated with lake shallowing. Salinities exceeded 10,000 μ S.cm⁻¹ for at least those parts of the time represented by Zones 27-28, 31, 33, 35 and 37 (Fig. 7), which likely reflect loss of overflow at these times and significant regressions given relatively low CA values and the repeated development of palaeosols at these times. Intermediate salinities of 3000–10,000 μS.cm⁻¹ developed during formation of Zones 30, 34, 36, 38, 39 and 40. Relatively fresh periods also prevailed through parts of Zones 32, 38 and 39.

CA Axis 1 suggests that water depths were mostly shallow to intermediate (Fig. 7). However, dominance by planktonic *A. granulata* and *A. agassizii* indicates three deeper water phases and several intermediate lake levels. The saline diatoms *T. faurii* and *T. rudolfi* are common in Zone 35 along with several benthic species, suggesting that the palaeolake was relatively shallow. Palaeosols continue to overprint aquatic deposits, confirming alternating episodes of exposure and flooding of the Koora Basin.

5.2.5. Unit V (83.5 ka to present; 27.0-0 m) and palaeolake termination

Unit V was augered due to its friable nature and consists of clayey silt and gravelly sand (F22, Table 1). Diatoms are rare and, where present, are dominated by *R. gibberula*, suggesting ephemeral wetlands in an otherwise terrestrial sequence. The observations are in line with a major lake regression.

The cessation of lacustrine deposition at the coring site

represents a major event in the palaeoenvironmental history of the Koora Basin. Hypsometric analysis based on the present basin morphology indicates that the last Koora paleolake could not have risen above 860 m, because this is the maximum elevation of the southwestern basin margin, assuming that the outlet has been relatively stable. The inferred paleolake would have extended over a north-south distance of ca. 35 km, was at least up to 86 m deep and hosted a minimum lake volume of 5.2 km³ (Fig. 8A-C). The ODP-OLO12-1A core location has a present elevation of 845 m, so the 860 m lake surface represents the last possible highstand when the core site was covered by the palaeolake. Field observations (Fig. 2C) and structure-from-motion elevation data reveal a shoreline presently at 890 m elevation on the eastern site of the basin margin (Fig. 2C). This shoreline indicates that the geometry of the Koora Basin has a complex history which involved normal faulting with a throw of at least 30 m between eastern and western basin margins. Hence, the hypsometric data are only applicable for the last stage of the Koora lake, but earlier lake phases may have had similar lake depths.

Fig. 8D—E shows north-south elevation profiles and their locations along the western margin and the central axial floor of the Koora Basin with an inferred lake level for about 80 ka. A lake at an elevation of 860 m resulted in overflow along a >5 km wide front over the southwestern trachyte horst towards Lake Magadi, which helps to explain the large lateral extent of a series of parallel sand and boulder bars previously attributed to a megaflood event (Figs. 2D and 8F; Baker, 1958; Marsden, 1979). This overflow elevation suggests that the minimum depth at the coring site when the last of the deep-water *Aulacoseira* assemblages were flourishing was about 42 m (Fig. 8D). At that time there may also have been inflow from a Palaeolake Kwenia into the north-eastern Koora Basin (Fig. 1).

Subsequently, an outlet was cut into the southwestern trachyte horst, which caused a significant lake level drop that resulted in the deposition of fluvial and ephemeral wetland deposits on top of Units I—IV at the ODP-OLO12-1A core site.

5.3. Regional correlations

Regional correlations between Koora, Lake Magadi and Olorgesailie are shown in Fig. 9. The Koora diatom CA reflects relative water depth with values > 0 representing deeper water (D1–D24). At Olorgesailie, outcrop evidence indicates terrestrial deposition and pedogenesis dominated prior to 750 ka (Potts et al., 2018; Behrensmeyer et al., 2018). The Koora diatom data indicate initially shallow to intermediate lakes with deeper water developing after about 870 ka (lakes L1 to L2, Fig. 9). Magadi pollen (HSPDP-MAG14-2A) are absent for earlier periods, but the presence of laminated sediments and authigenic carbonates (Owen et al., 2019) indicates fresh to moderately saline lakes from 1000 to 725 ka. Subsequently, the Koora lakes L3–L4 (~725–475 ka) coexisted with intermittent and expansive freshwater lakes at Olorgesailie during a period when mainly positive Magadi pollen PCA data suggest generally wetter conditions.

Olorgesailie environmental data for the 500—320 ka period is missing due to erosion, but is preserved at Koora and Magadi. Periods with negative values in the Magadi pollen data (Fig. 9) reflect increases in *Acacia (Vachellia)*, other forest taxa and herbaceous plants, combined with decreases in Cyperaceae and *Podocarpus* (Owen et al., 2018), suggesting drier phases. Planktonic diatom percentages from Lake Magadi (Owen et al., 2018, 2019) indicate high variability between about 580 and 300 ka, with diatoms disappearing at times when the Koora Basin was dry or occupied by shallow lakes. Calcretes capping the Oloronga Beds at Magadi are poorly dated, but likely formed after 440 ka (Owen et al., 2019) and

reflect a major regression towards the Magadi core site. They are favoured by dry conditions and their development likely correlates with a drier phase between D14 and D15 in the ODP-OLO12-1A record (Fig. 9).

After ~400 ka, the Koora and Magadi records diverge. At the MAG14-2A site (Fig. 1B), the Magadi Basin was occupied by a lake or waterlogged mudflats with anoxic bottom water/sediment for most of the time, which allowed pollen and organic matter to be preserved, facilitated the growth of pyrite in mud and prevented the formation of palaeosols, although rare mudcracks suggest minor exposure. This major contrast with the repeated appearance and disappearance of lakes (D15–D24) at Koora likely reflects Magadi's location in the depocentre of the southern Kenya Rift, towards which surface- and groundwaters flow southwards via numerous faults resulting in a tectonic sump (Becht et al., 2006). Nasikie Engida, a small permanent saline lake northeast of Lake Magadi is, for example, maintained today by springs (Renaut et al., 2021), as are several lagoons around modern ephemeral Lake Magadi, whereas the Koora Basin is dry.

The Magadi diatom PCA Axis 1 shows a series of peaks with decreasing amplitude (F1-F10, Fig. 9) that, given potential dating errors, broadly overlap Koora evidence for higher lake levels (D15-D24) and wetter conditions. Owen et al. (2018) noted that the Magadi peaks reflect inputs of freshwater benthic diatoms to a permanent saline lake delivered by flood events, which is consistent with the Koora CA data for intermittent wetter conditions. Interestingly, the best example of correspondence between these datasets (peaks of D17-D18 and adjacent troughs with F3) is between 375 and 275 ka, which also correspond with the most precise $^{40}\mathrm{Ar}/^{39}\mathrm{Ar}$ dating in the Magadi core. In contrast, Magadi peaks F6 and F7 do not appear to correlate with deep phases at Koora, but there are small positive excursions within a broadly shallow-water phase. D19 does not appear to correlate with any peak in the Magadi data. This high lake level appears to be a relatively short event and its absence at Magadi might simply reflect differences in sampling intervals.

5.4. Climate correlations and tectonic controls

Sedimentary basins in the south Kenya Rift document environmental changes through the last million years that reflect both tectonic and climatic change. Insolation forcing of East African precipitation has been suggested by several researchers (Kutzbach and Otto-Bliesner, 1982; deMenocal, 1995) with models relating northward expansions of summer monsoon rainfall to orbitally forced increases in northern summer insolation, and perhaps contributions from Mediterranean-sourced winter rains in northern East Africa. These relationships have been explored in some detail by Kutzbach et al. (2020) who modelled the impacts of changing greenhouse gasses, ice sheet volumes and orbital parameters, including axial precession, tilt and orbital eccentricity. Within the tropical zone, which encompasses the Koora Basin, they noted that equatorial rains were likely ~10-15 % lower during glacial periods, when CO₂, tropical temperatures, and convection were all lower.

The diatom record from ODP-OLO12-1A provides an opportunity to compare equatorial lake level change and global climate records (Fig. 10). The last one-million years have been associated with large variations in the scale and timing of glacial-interglacial climates. Both marine and lake records (Lisiecki and Raymo, 2005; Clark et al., 2006; Johnson et al., 2016) suggest changes in the dominant climate periodicities from an obliquity-controlled 41 ka cycle to an eccentricity-controlled 100 ka cycle, a period that has been referred to as the Mid-Pleistocene Transition (MPT) (Tziperman and Gildor, 2003). The MPT has been generally placed

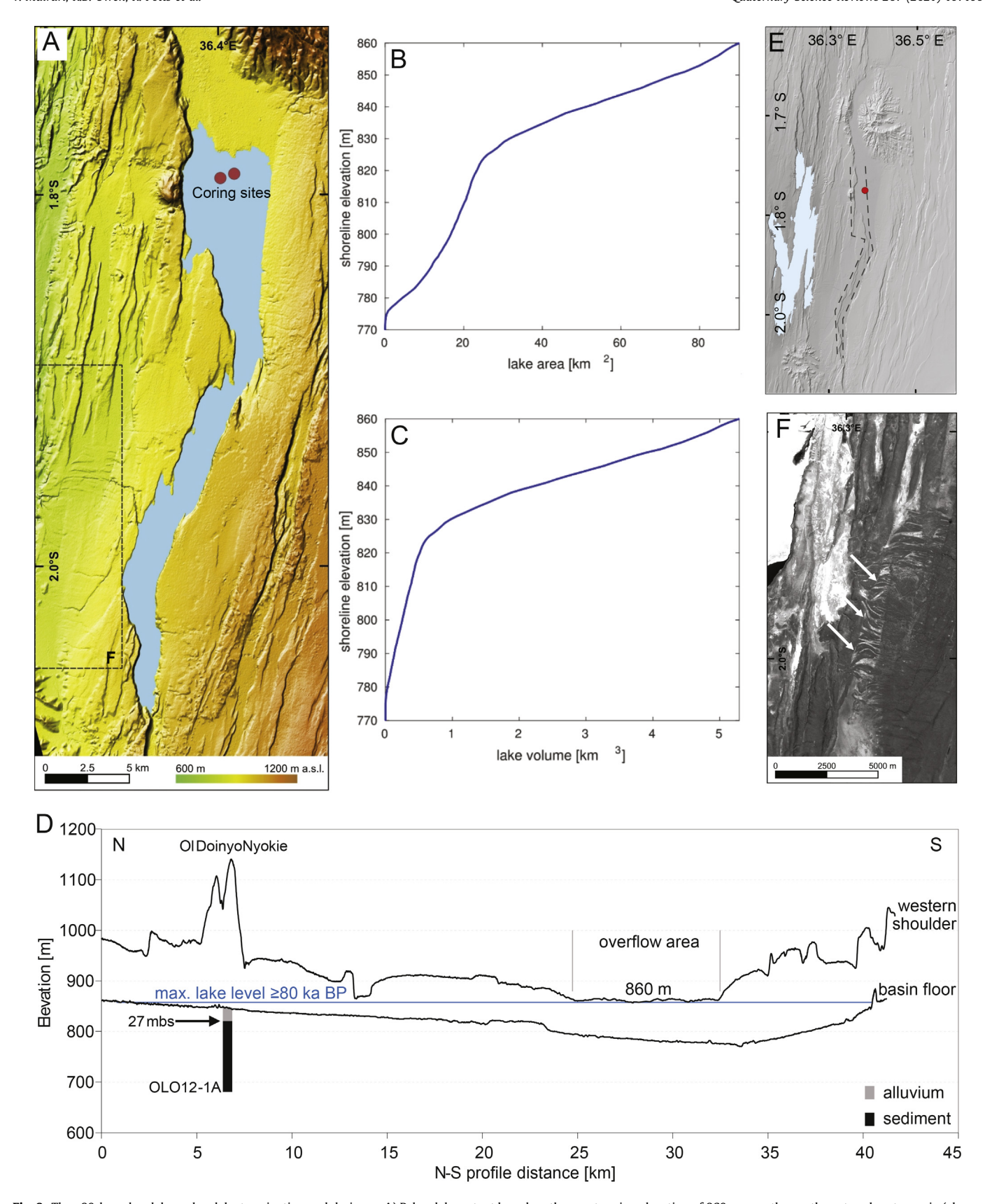


Fig. 8. The ~80-ka palaeolake, palaeolake termination and drainage. A) Palaeolake extent based on the overtopping elevation of 860 m over the southwestern horst margin (shown in "D"). B—C) Hypsometric analysis based on the modern basin topography from a SRTM-30 m digital elevation model, indicating lake area and volume for differing shoreline elevations. D) N—S elevation profiles, shown in "E", extracted from the 5 m ALOS Global Digital Elevation Model. Lake depth at the coring location was ca. 37 m. Subsequent outlet erosion caused a lake level fall and lake retreat from the coring site that led to alluvial deposition on top of the lacustrine sediments of Units I—IV. E) Transect lines in "D". F) Panchromatic optical image showing boulder bars (white arrows) formed by overtopping of the southwestern horst margin of the Koora Basin. Area partially shown in "A" would have drained to Lake Magadi further west.

between 1250 and 700 ka (Clark et al., 2006). Based on an ¹⁸O stable isotope record from marine foraminifera, Crundwell et al. (2008) defined four stages (Fig. 10) and recognised the early-MPT as starting only at ~870 ka (Fig. 9). Head and Gibbard (2015) noted major changes at about 900 ka in marine biota and environment. Evidence of similar changes in Africa have been less clear. However, a variety of proxies from Lake Malawi sediments suggest significant environmental change after ~800 ka (Ivory et al., 2016) and ~900 ka (Johnson et al., 2016) that may reflect either tectonic shifts in accommodation space and/or a transformation from variable and drier climates to more humid conditions. A recent Koora bulk organic carbon isotope (¹³C_{OM}) record from core OLO12-1A also shows a shift towards more positive values after 790 ka, suggesting higher C₄-plant dominance in the vegetation near the end of the MPT (Lupien et al., 2021).

The Koora diatom CA record (Fig. 10) reflects changes in relative water depth and is viewed here in the context of the MPT subdivision of Crundwell et al. (2008). Fig. 10 also shows the diatom proxy data with associated age uncertainties along the y-axis (Potts et al., 2020). These age uncertainties complicate comparisons, particularly in the lower core where there are relatively large temporal sampling gaps. Potts et al. (2020), for example, noted that only 11 % of the variation in the CA axis of the entire core-record followed orbital cyclicity. However, the low detection of orbital cyclicity could be due in part to the low sampling resolution in the early part of the record (>500 ka), which limits identifying precessional frequencies.

Deeper lakes are represented by more positive CA values, which variably correlate with some of the negative excursions in the ¹⁸O benthic stack data that document interglacial episodes (Lisiecki and Raymo, 2005). During the pre-MPT period, the Koora lakes were shallow and fresh with small CA peaks (D1-3, Fig. 10) that overlap with less pronounced interglacials (MIS 28b, 27 and 25e, Fig. 10). No equivalent to MIS 23c was recognised, although sampling in this part of the Koora core is of low resolution and may not pick this out. The onset of the early-MPT in the Koora Basin experienced a major palaeolake deepening at ~870–850 ka and the formation of a later series of freshwater lakes that continued through much of the next 350 kyr. Although age uncertainties are large (Fig. 10) and samples are few in this part of the core, this deepening (D4) could suggest response to an increase in the intensity of interglacials with MIS 21g. Through the remaining early and late MPT, correlations are generally poor with relatively deep lakes (D5-D14) prevailing, except for major regressions between D5 and D6, where the B-M boundary also improves age model accuracy. Other notable regressions took place between D6 and D7 and D11 and D12, but with lakes remaining deep even during the glacial MIS16a.

A major shallowing took place at ~470—390 ka, around the time of the Mid-Brunhes Event (MBE) at ~430 ka, which represents a climate transition towards higher amplitude glacial-interglacial variation (EPICA Community Members, 2004). The MBE also partially overlaps with Marine Isotope Stage 11 (424—374 ka), the longest and warmest interglacial of the last half million years (Howard, 1997). During post-MPT times, lakes were comparatively more variable than the benthic ¹⁸O record, but with several events that show good correlation with the marine record (9c/e and D17—18; 5e and D23; 5a and D24). The core does not preserve sediments equivalent to MIS1—4.

The three south Kenya Rift basins show broad similarities in environmental variability with all suggesting: 1) relatively low lakes or stable land surfaces during the Pre-MPT, 2) evidence for wetter conditions and higher lakes at least between about 750 and 500 ka, 3) lower lakes and drier conditions or erosion (Olorgesailie) around the Mid Brunhes Event, followed by 4) variable conditions through the Post MPT. These comparisons suggest that Pleistocene

global climate change affected the southern Kenya Rift, but also that other factors such as regional to local tectonic controls are also represented in the lake depth cycles of the different basins.

Lake fluctuations that do not correspond to global climate patterns could reflect tectonic controls at the local basin scale. Accommodation space, for example, was initiated by grid faulting. which fractured the underlying Magadi Trachyte Formation into a series of north-south horsts and grabens. Baker and Mitchell (1976) suggested that fault activity developed progressively with three phases of displacement highlighted at about 1300, 900-600 and 400-240 ka. Magadi and Koora drilling evidence indicate that the basal trachytes are essentially identical in age, with these flood lavas extending to Olorgesailie. So, this region was essentially flattened by flood volcanism, but soon thereafter the area was subdivided by faulting, probably co-genetic with the volcanism. Owen et al. (2019) also noted that loss of transition metals in their Lake Magadi core likely reflected drainage diversion at about 540 ka in the western part of the south Kenya Rift, suggesting an additional phase of faulting, close to the onset of erosion at Olorgesailie.

Drainage changes may also impact the lake level record. Today, the major source of water to the Koora Plain is from the Ol Keju Nyiro River, which drains areas to the north and the eastern rift margin. The latter area is crossed by a series of tributaries that merge to form a single river that turns north to the Oltepsei Plain at "Lc. 2" in Fig. 1A. Speculatively, past fault movements, or autocyclic avulsion, could have led to the former river switching to a southward route to the neighbouring Kwenia Basin (east of the Koora Plain, Fig. 1A), potentially interrupting water supplies to the Koora Basin, although during wetter periods overflow into the Koora Basin near Oolkululu (Lc.1, Fig. 1A) may have re-established hydrological connectivity. Similar switching processes have been noted from Summer Lake and Lake Abert in the US Basin and Range (Davis, 1985). Evidence for complex drainage changes has also been reported by Marsden (1979), who noted that there are several wind and water gaps cutting through horst blocks, implying that parts of the drainage system may predate grid faulting.

Volcanism can also affect accommodation space through the infilling of basins. Sedimentation rates have clearly varied through the last million years at Koora with major increases taking place during Unit III times (~255–212 ka) due to increased inputs of tephra (Deino et al., 2019).

5.5. Late quaternary environments and hominins

Potts et al. (2020) synthesised environmental data from multiple records in ODP-OLO12-1A that suggested considerable environmental variability beginning by around 400 ka. This phase of variability lies within the 500 to 320 ka interval at Olorgesailie, during which a major change from Acheulean to Middle Stone Age tools took place, and also includes a period of major mammal turnover. Potts et al. (2020) framed their discussion of hominins in terms of resource landscapes and how these affected ecological dynamics, reporting that diatom taxonomic variability changed considerably through the last million years.

Prior to 425 ka, diatom interassemblage variability was relatively low (Potts et al., 2020). The diatom transfer function data reported here provide greater detail on the aquatic resources through this period, indicating relatively low pH (~7–9) and conductivities (<1000 μ S.cm⁻¹), with only six samples suggesting values rising above 10,000 μ S.cm⁻¹. Interassemblage diatom variability increased between 425 and 350 ka (Potts et al., 2020), reflecting greater temporal habitat change (shallow to deep lakes), with pH (8–10) and conductivity (<500 to 12,000 μ S.cm⁻¹) values also trending slightly higher, which would have impacted hominins given that modern humans have an upper limit for potable water of

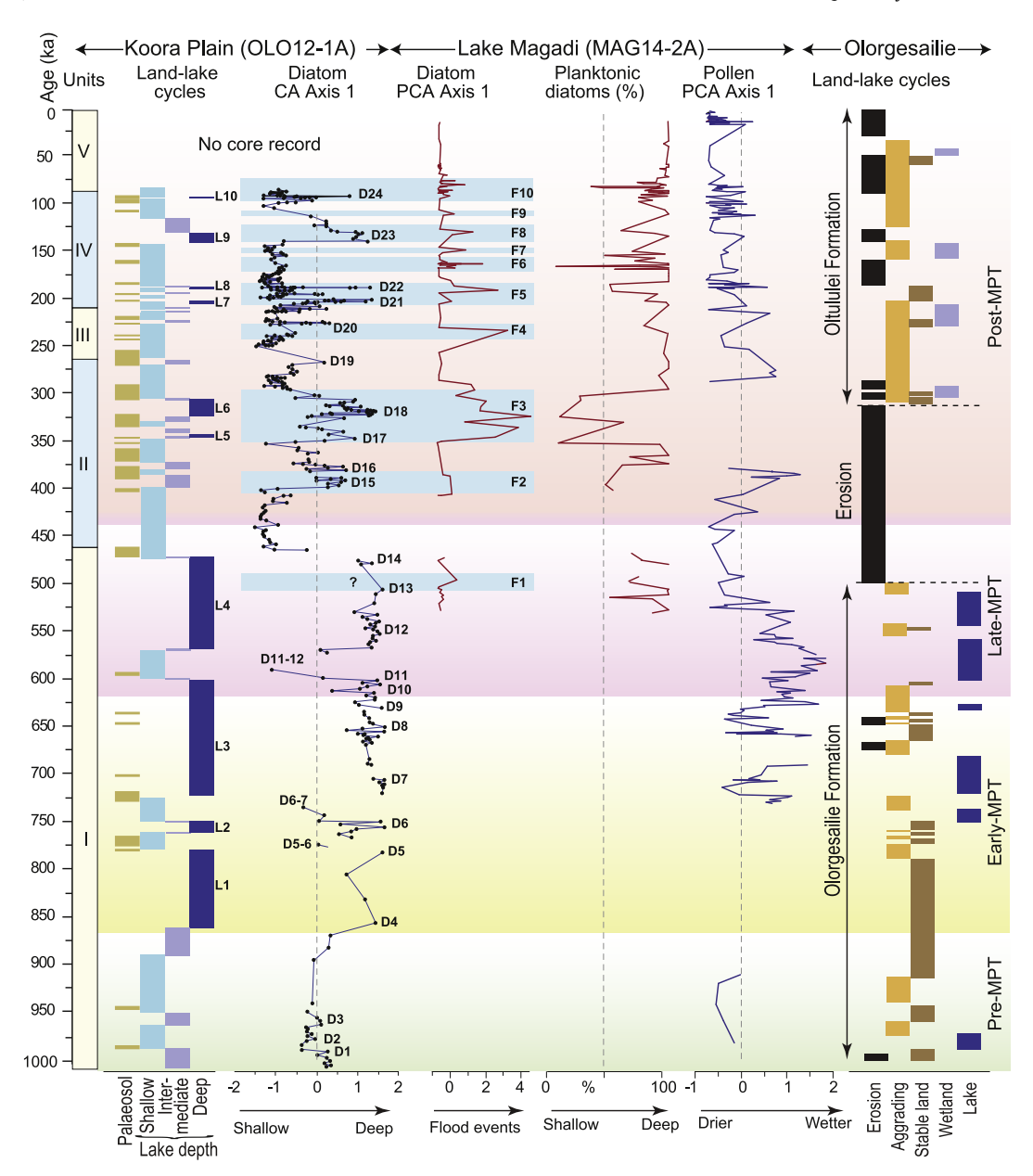


Fig. 9. Environmental change across the south Kenya Rift. Palaeosols after Potts et al. (2020) showing increasing lake desiccation events upwards. Land-lake cycles based on PCA scores in diatom CA Axis 1 (to right). Deeper lakes reflect values > 0.75; intermediate lakes = 0-0.75; shallow lakes = <0, distinguishing ten deep lakes (L1-L10). Magadi diatom PCA (Owen et al., 2018) reflects input of benthic freshwater diatoms to a saline lake and thus flooding events. Magadi pollen show long term reduction in PCA values, reflecting an overall decrease in moisture, but with many wetter intervals. Olorgesailie land-lake cycles after Potts et al. (2018). Early-, late- and post-Mid-Pleistocene Transition (MPT) boundaries as defined by Crundwell et al. (2008).

only about 2500 μ S.cm⁻¹ (Potts et al., 2020). Variability in water resources peaked during the subsequent 270 kyr with lakes deepening and shallowing many times along with variations in conductivity (<500 to >16,000 μ S.cm⁻¹) and pH (7.5–10.5).

These changing environments would have exerted considerable pressures on hominin ecological interactions as posited by Potts et al. (2020). Lakes alternated between fresh and saline status many times, which may have forced hominin groups to periodically rely on rivers and springs for potable water (Barboni et al., 2019) or perhaps to disperse elsewhere. For example, a major lake shallowing between 470 and 390 ka suggests drier conditions that would have changed the resource base for hominins in the region.

Major environmental changes started with the onset of the early-MPT and were partly driven by global climate. The 470–390

shallowing event may also reflect a global climate link, at least in part, given that it overlaps with the warmest interglacial since the onset of the late-MPT. This event was followed by increased environmental variability, with lakes rapidly filling their basins only to repeatedly dry out again. However, departures from these influences are shown by lakes remaining high during some high δ^{18} O intervals, suggesting regional-scale tectonic and/or volcanic impacts (changing topography and lake basin geometry, drainage diversions, volcanic damming) on local environments and hominin resources. Consequently, understanding environmental variability and the evolutionary pressures that these changes exerted on hominins in the Koora, Magadi and Olorgesailie basins requires a consideration of three different potential controls - global climate, regional tectonism and volcanic activity. Changes in moisture

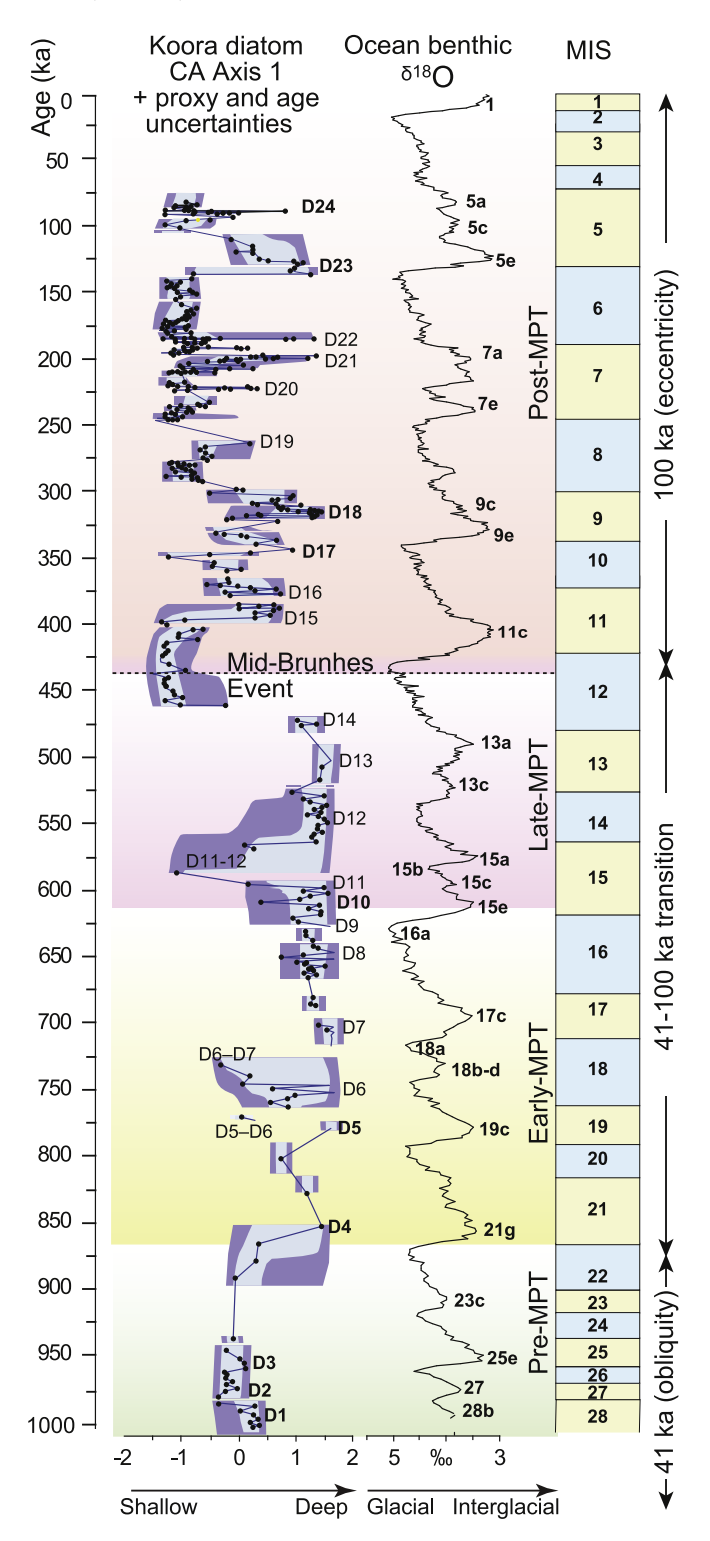


Fig. 10. Comparison of Koora deep water phases with the global climate record. Note deeper-water peaks (D1–D24), several of which correlate with labelled interglacial stages in the benthic foraminiferal oceanic δ^{18} O record (to right), but with others that do not. Good correlations discussed in text shown in bold. ¹⁸O data after Lisickie and Raymo (2005) with MIS labelling after Railsback et al. (2015). Age model uncertainty shown along y-axis. The x-axis shows analytical uncertainty (after Potts et al., 2020). Purple (darker) envelopes reflect 68 % confidence interval with bluey-grey (lighter) indicating 95 % confidence, based on analytical and age model errors (Deino et al., 2019). (For interpretation of the references to colour in this figure legend, the reader is referred to the Web version of this article.)

availability and climate variability, combined with a tectonically modified landscape, exerted significant pressures on resources and ecological interactions that, in turn, could have led to significant selective/adaptive pressures on our human ancestors.

6. Conclusions

Diatoms in the Koora Basin document a one-million-year history of environmental change that reflects global climate controls, regional rifting and volcanism. Some environmental changes correlate in time with glacial-interglacial stages, but others do not. The palaeolakes in the Koora Basin were shallow and fresh between 1000 and 870 ka. Fresh and generally deeper lakes prevailed between 870 and 470 ka. A major lake shallowing took place between 470 and 390 ka, reflecting a decrease in moisture availability corresponding in part to a marked global interglacial to glacial transition (mid-Brunhes Event). This was followed by highly variable conditions with lakes rapidly expanding, contracting and desiccating through to the top of the core record at ~83 ka. Koora mineralogical data also confirm a trend towards saline lakes and variable moisture availability after ~470 ka as do increasingly frequent episodes of pedogenesis.

The periodic development of extensive freshwater lakes at Olorgesailie after about 750 ka broadly correlates with the appearance of extensive lakes in both the Koora and Magadi basins. Subsequent changes in the Koora palaeolake are reflected across the south Kenya Rift with sedimentological, mineralogical and diatom evidence indicating that the lake at Magadi trended towards increasing salinity reflecting a long-term change to drier conditions. At Magadi, diatoms record a post-500 ka record that shows that a lake or shallow mudflats were continuously present and probably supported by springs at times when the Koora Basin was dry. However, benthic diatoms suggest multiple flood events that correlate with high Koora lake levels that signify wetter periods. Magadi pollen also indicate floral changes in the south Kenya Rift that indicate broadly drier conditions, interrupted by wetter intervals, after about 500 ka.

The changes in the Koora Basin and other parts of the south Kenya Rift were driven by global climate changes, regional tectonism and volcanism, producing a complex landscape with relatively moist settings replaced by generally drier conditions with wetter intervals during and after the Mid-Brunhes Event. These changes with their impacts on ecological resources may help to explain faunal extinctions and a major change from Acheulean to MSA artefacts that required adaptation to an increasingly complex resource base.

Author contributions

VM and RBO conceptualised the diatom-based study, carried out diatom analyses and wrote the manuscript with support from RD and SR. RP and AKB selected the drilling location and supervised field work. SR and RD contributed survey data, hypsometric analysis and analysis of the palaeolake termination. ALD and RD provided chronological aspects of the research. EJB provided palaeosol data. NR and DD provided mineralogical data. KBS, RD and AN provided field and laboratory support. All authors contributed to discussion, editorial work and interpretations.

Declaration of competing interest

The authors declare that they have no known competing financial interests or personal relationships that could have appeared to influence the work reported in this paper.

Acknowledgements

This research was supported by the National Museums of Kenya, the Oldonyo Nyokie Group Ranch, and the Olorgesailie field team led by I.M. Nume and I.N. Mativo, Research and drilling permits were provided by the Kenvan National Council for Science and Technology, the Kenyan Ministry of Mines, and the National Environmental Management Authority of Kenya, DOSECC Exploration Services supervised drilling by Drilling and Prospecting International (DPI). The LacCore and CSDCO facilities (University of Minnesota) assisted with core handling, processing and storage. Funding was provided by the Peter Buck Fund for Human Origins Research (Smithsonian), the William H. Donner Foundation (R.P.), the Ruth and Vernon Taylor Foundation (R.P.), Whitney and Betty MacMillan (R.P.), National Science Foundation grants EAR 1322017 (A.L.D.) and EAR 1349599 (D.D.), a Smithsonian Postdoctoral Fellowship and the Geo. X - Research Network for Geosciences in Berlin and Potsdam (R.D.), the Swiss National Science Foundation grant P300P2 158501 (M.S.), and the Smithsonian's Human Origins Program (R.P). The Hong Kong Research Grants Council provided funding for diatom studies of the core material.

Appendix A. Supplementary data

Supplementary data to this article can be found online at https://doi.org/10.1016/j.quascirev.2021.107106.

References

- Baker, B.H., 1958. Geology of the Magadi area. Geol. Surv. Kenya Rep. 42.
- Baker, B.H., 1986. Tectonics and volcanism of the southern Kenya Rift Valley and its influence on rift sedimentation. In: Frostick, L.E., Renaut, R.W., Reid, I., Tiercelin, J.J. (Eds.), Sedimentation in the African Rifts, vol. 25. Geol. Soc. Lond. Spec. Publ., pp. 45–58
- Baker, B.H., Mitchell, J.G., 1976. Volcanic stratigraphy and geochronology of the Kedong-Olorgesailie area and the evolution of the south Kenya Rift Valley. J. Geol. Soc. Lond. 132, 467–484.
- Barboni, D., Ashley, G.M., Bourel, B., Arráiz, H., Mazur, J.-C., 2019. Springs, palm groves, and the record of early hominins in Africa. Rev. Palaeobot. Palynol. 266, 23–41
- Barker, P., Gasse, F., Roberts, N., Taieb, M., 1990. Taphonomy and diagenesis in diatom assemblages; a Late Pleistocene palaeoecological study from Lake Magadi, Kenya. Hydrobiologia 214, 267–272.
- Battarbee, R.W., Kneen, M.J., 1982. The use of electronically counted microspheres in absolute diatom analysis. Limnol. Oceanogr. 27, 184–188.
- Battarbee, R.W., Juggins, S., Gasse, F., Anderson, N.J., Bennion, H., Cameron, N., 1998. European Diatom Database (EDDI): an information system for palae-oenvironmental reconstruction. In: European Climate Science Conference, Vienna. 19-23. October 1998.
- Becht, R., Mwango, F., Muno, F.A., 2006. Groundwater links between Kenyan rift valley lakes. In: Odada, E., Olago, D., Ochola, W., Ntiba, M., Wandiga, S., Gichuki, N., Oyieke, H. (Eds.), Proc. 11th World Lake Congr., Nairobi, 31 October-4th November, 2005, vol. 2. Ministry of Water and Irrigation - International Lake Environment Committee (ILEC), Nairobi, pp. 7–14.
- Behr, H.-J., 2002. Magadiite and Magadi-chert: a critical analysis of the silica sediments in the Lake Magadi. In: Renaut, R.W., Ashley, G.M. (Eds.), Sedimentation in Continental Rifts, vol. 73. SEPM Special Publication, pp. 257–273.
- Behrensmeyer, A.K., Potts, R., Deino, A., 2018. The Oltulelei Formation of the southern Kenyan Rift Valley: a chronicle of rapid landscape transformation over the last 500 k. y. Geol. Soc. Amer. Bull. 130, 1474–1492.
- Behrensmeyer, A., Potts, R., Deino, A., Ditchfield, P., 2002. Olorgesailie, Kenya: a million years in the life of a rift basin. In: Renaut, R.W., Ashley, G. (Eds.), Sedimentation in Continental Rifts, vol. 73. SEPM Specl. Publication, pp. 97–106.
- Brooks, A.S., Yellen, J.E., Potts, R., Behrensmeyer, A.K., Deino, A.L., Leslie, D.E., Ambrose, S.H., Ferguson, J.R., d'Errico, F., Zipkin, A.M., Whittaker, S., Post, J., Veatch, E.G., Foecke, K., Clark, J.B., 2018. Long-distance stone transport and pigment use in the earliest Middle Stone Age. Science 360, 90–94.
- Busk, H.G., 1939. Explanatory note on the block diagram of the great rift valley from Nakuru to Lake Magadi (plate XIV). Quart. J. Geol. Soc. 95 (1–4), 231–233.
- Campisano, C.J., Cohen, A.S., Arrowsmith, J.R., Asrat, A., Behrensmeyer, A.K., Brown, E.T., Deino, A.L., Deocampo, D.M., Feibel, C.S., Kingston, J.D., Lamb, H.F., Lowenstein, T.K., Noren, A., Olago, D.O., Owen, R.B., Pelletier, J.D., Potts, R., Reed, K.E., Renaut, R.W., Russell, J.M., Russell, J.L., Schäbitz, F., Stone, J.R., Trauth, M.H., Wynn, J.G., 2017. The Hominin Sites and Paleolakes Drilling Project: acquiring high-resolution paleoclimate records from the East African

- Rift System and their implications for understanding the environmental context of Hominin evolution. PaleoAnthropology 1–43. https://doi.org/10.4207/PA.2017.ART104.
- Clark, P.U., Archer, D., Pollard, D., Blum, J.D., Rial, J.A., Brovkin, V., Mix, A.C., Pisias, N.G., Roy, M., 2006. The middle Pleistocene transition: characteristics, mechanisms, and implications for long-term changes in atmospheric pCO₂. Ouat. Sci. Rev. 25, 3150–3184.
- Cohen, A., Arrowsmith, R., Behrensmeyer, A., Campisano, C., Feibel, C., Fisseha, S., Johnson, R., Dedaso, Z., Lockwood, C., Mbua, E., Olago, D., Potts, R., Reed, K., Renaut, R., Tiercelin, J.-J., Umer, M., 2009. Understanding paleoclimate and human evolution through the hominin sites and paleolakes drilling project. Sci. Drill. 8, 60–65.
- Cohen, A., Campisano, C., Arrowsmith, R., Asrat, A., Behrensmeyer, A.K., Deino, A., Feibel, Hill A., Johnson, R., Kingston, J., Lamb, H., Lowenstein, T., Noren, A., Olago, D., Owen, R.B., Potts, R., Reed, K., Renaut, R., Schäbitz, F., Tiercelin, J.-J., Trauth, M., Wynn, J., Ivory, S., Brady, C., O'Grady, R., Rodysill, J., Githiri, J., Russell, J., Foerster, V., Dommain, R., Rucina, S., Deocampo, D., Billingsley, A., Beck, C., Dullo, L., Feary, D., Garello, D., Johnson, T., Junginger, A., Karanja, M., Kimburi, E., Mbuthia, A., McCartney, T., McNulty, E., Muiruri, V., Nambiro, E., Njagi, D., Norman, J., Rabideaux, N., Raub, T., Sier, M., Smith, P., Urban, J., Warren, M., Wondiymu, E., Yost, C., 2016. The hominin sites and paleolakes drilling project: inferring the environmental context of human evolution from Eastern African rift lake deposits. Sci. Drill. 21, 1–16.
- Crossley, R., 1976. Structure, Stratigraphy and Volcanism in the Nguruman Escarpment Area of the Western Side of the Kenya Rift Valley. PhD thesis. University of Lancaster, p. 297.
- Crundwell, M., Scott, G., Naish, T., Carter, L., 2008. Glacial—interglacial ocean climate variability from planktonic foraminifera during the Mid-Pleistocene transition in the temperate Southwest Pacific, ODP Site 1123. Palaeogeogr. Palaeoclimatol. Palaeoecol. 260, 202–229.
- Davis, J.O., 1985. Correlation of late Quaternary tephra layers in a long pluvial sequence near Summer Lake, Oregon. Quat. Res. . 23, 38–53.
- Deino, A.L., Dommain, R., Keller, C.B., Potts, R., Behrensmeyer, A.K., Beverly, E.J., King, J., Heil, C.W., Stockhecke, M., Brown, E.T., Moerman, J., deMenocal, P., The Olorgesailie Drilling Project, Team, 2019. Chronostratigraphic model of a high-resolution drill core record of the past million years from the Koora Basin, south Kenya Rift: overcoming the difficulties of variable sedimentation rate and hiatuses. Quat. Sci. Rev. 215, 213–231.
- Deino, A., Potts, R., 1990. Single-crystal 40Ar/39Ar dating of the Olorgesailie Formation, southern Kenya rift. J. Geophys. Res. 95, 8453–8470.
- deMenocal, P., 1995. Plio-pleistocene african climate. Science 270, 53-59.
- deMenocal, P., 2004. African climate change and faunal evolution during the Pliocene-Pleistocene. Earth Planet Sci. Lett. 220, 3—24.
- EPICA community members, 2004. Eight glacial cycles from an Antarctic ice core. Nature 429, 623–628.
- Eugster, H.P., 1980. Lake Magadi, Kenya and its precursors. In: Nissenbaum, A. (Ed.), Hypersaline Brines and Evaporites. Elsevier, Amsterdam, pp. 195–232.
- Faith, J.T., Du, A., Behrensmeyer, A.K., Davies, B., Patterson, D.B., Rowan, J., Wood, B., 2021. Rethinking the ecological drivers of hominin evolution. Trends Ecol. Evol. https://doi.org/10.1016/j.tree.2021.04.011.
- Felske, G.N., 2016. Genesis of Calcretes and Related Carbonate Rocks in the Southern Kenya Rift. MSc dissertation, University of Saskatchewan 170pp.
- Gasse, F., 1986. East African Diatoms: Taxonomy. Ecological Distribution. Cramer, Stuttgart 201pp, p. 63.
- Gasse, F., 1987. Diatoms for reconstructing palaeoenvironments and paleohydrology in tropical semi-arid zones. Hydrobiologia 154, 127–163.
- Gasse, F., Juggins, S., Ben Khelifa, L., 1995. Diatom-based transfer functions for inferring past hydrochemical characteristics of African lakes. Palaeogeogr. Palaeoclimatol. Palaeoecol. 117, 31–54.
- Goetz, C., Hillaire-Marcel, C., 1992. U-series disequilibria in early diagenetic minerals from Lake Magadi sediments: dating potential. Geochem. Cosmochim. Acta 56, 1331–1341.
- Guiry, M.D., Guiry, G.M., 2021. AlgaeBase. World-wide Electronic Publication. National University of Ireland, Galway searched in July 2021s. https://www.algaebase.org.
- Guth, A., 2014. Geological map of the southern Kenya Rift. Geol. Soc. Am. Dig. Map Chart Ser. DMCH016.
- Hammer, Ø., Harper, D.A.T., Ryan, P.D., 2001. PAST: paleontological Statistics software package for education and data analysis. Paleontol. Electron. 4, 9.
- Head, M.J., Gibbard, P.L., 2015. Early—Middle Pleistocene transitions: linking terrestrial and marine realms. Quat. Int. 389, 7–46.
- Hillaire-Marcel, C., Casanova, J., 1987. Isotopic hydrology and paleohydrology of the Madagi (Kenya)-Natron (Tanzania) basin during the late Quaternary. Palaeogeogr. Palaeoclimatol. Palaeoecol. 58, 155–181.
- Howard, W.R., 1997. A warm future in the past. Nature 388, 418–419.
- Hublin, J.-J., Ben-Ncer, A., Bailey, S.E., Freidline, S.E., Neubauer, S., Skinner, M.M., Bergmann, I., Le Cabec, A., Benazzi, S., Harvati, K., Gunz, P., 2017. New fossils from Jebel Irhoud, Morocco and the pan-African origin of *Homo sapiens*. Nature 546, 289—292.
- Ivory, S.J., Blome, M.W., King, J.W., Mcglue, M.M., Cole, J.E., Cohen, A.S., 2016. Environmental change explains cichlid adaptive radiation at Lake Malawi over the past 1.2 million years. Proc. Natl. Acad. Sci. Unit. States Am. 113, 11895—11900.
- Jirsa, F., Gruber, M., Stojanovic, A., Omondi, S.O., Mader, D., 2013. Major and trace element geochemistry of Lake Bogoria and Lake Nakuru, Kenya, during extreme

- draught. Chem. Erde 73, 275-282.
- Johnson, T.C., Werne, J.P., Brown, E.T., Abott, A., Berke, M., Steinman, B.A., Halbur, J., Contreras, S., Grosshuesch, S., Deino, A.L., Lyons, R.P., Scholz, C.A., Schouten, S., Sinninghe Damsté, J.S., 2016. Progressively wetter climate in southern East Africa over the past 1.3 million years. Nature 537, 220–224.
- Juggins, S., 2007. C2 Software for Ecological and Palaeoecological Data Analysis and Visualisation. University of Newcastle, Newcastle-upon-Tyne. User Guide Version 1.5. https://www.staff.ncl.ac.uk/stephen.juggins/software/code/C2.pdf.
- Kelts, K., Hsü, K.J., 1978. Freshwater carbonate sedimentation. In: Lerman, A. (Ed.), Lakes. Springer, New York, pp. 295–353.
- Kilham, S.S., Kilham, P., 1975. *Melosira granulata* (EHR.) Ralfs: morphology and ecology of a cosmopolitan freshwater diatom. Verh. Internat. Verein. Limnol. 19, 2716—2721.
- Krammer, K., Lange-Bertalot, H., 1986. Bacillariophyceae 1. Naviculaceae. In: Ettl, H., Gerloff, J., Heynig, H., Mollenhauer, D. (Eds.), Süsswasserflora von Mitteleuropa. Fisher. Stuttgart. 2/1. p. 876.
- Krammer, K., Lange-Bertalot, H., 1988. Bacillariophyceae 2. Epithemiaceae. In: Ettl, H., Gerloff, J., Heynig, H., Mollenhauer, D. (Eds.), Süsswasserflora von Mitteleuropa. Fisher, Stuttgart 2/2, p. 596.
- Krammer, K., Lange-Bertalot, H., 1991a. Bacillariophyceae 3. Centrales, fragilariaceae, eunotiaceae. In: Ettl, H., Gerloff, J., Heynig, H., Mollenhauer, D. (Eds.), Süsswasserflora von Mitteleuropa. Fisher, Stuttgart, 2/3, p. 576.
- Krammer, K., Lange-Bertalot, H., 1991b. Bacillariophyceae 4. Achnanthaceae. In: Ettl, H., Gerloff, J., Heynig, H., Mollenhauer, D. (Eds.), Süsswasserflora von Mitteleuropa. Fisher, Stuttgart 2/4, p. 437.
- Kutzbach, J.E., Guan, J., He, F., Cohen, A.S., Orland, I.J., Chen, G., 2020. African climate response to orbital and glacial forcing in 140,000-y simulation with implications for early modern human environments. Proc. Natl. Acad. Sci. Unit. States Am. 117. 2255–2264.
- Kutzbach, J.E., Otto-Bliesner, B.L., 1982. The sensitivity of the African-Asian monsoonal climate to orbital parameter changes for 9000 years BP in a lowresolution general-circulation model. J. Atmos. Sci. 39, 1177–1188.
- Lee, R.K.L., Owen, R.B., Renaut, R.W., Behrensmeyer, A.K., Potts, R., Sharp, W.D., 2013. Facies, geochemistry and diatoms of late Pleistocene Olorgesailie tufas, southern Kenya Rift. Palaeogeogr. Palaeoclimatol. Palaeoecol. 374, 197–217.
- Legesse, D., Gasse, F., Radakovitch, O., Vallet-Coulomb, C., Bonnefille, R., Verschuren, D., Gibert, E., Barker, P., 2002. Environmental changes in a tropical lake (Lake Abiyata, Ethiopia) during recent centuries. Palaeogeogr. Palaeoclimatol. Palaeoecol. 187, 233–258.
- Lisiecki, L.E., Raymo, M.E., 2005. A Pliocene-Pleistocene stack of 57 globally distributed benthic δ18O records. Paleoceanography 20, PA1003. https:// doi.org/10.1029/2004PA001071.
- Lupien, R.L., Russell, J.M., Subramanian, A., Kinyanjui, R., Beverly, E.J., Uno, K.T., de Menocal, P., Dommain, R., Potts, R., 2021. Eastern African environmental variation and its role in the evolution and cultural change of *Homo* over the last 1 million years. J. Hum. Evol. 157, 103028. https://doi.org/10.1016/j.jhevol.2021.103028.
- Marsden, M., 1979. Origin and Evolution of the Pleistocene Olorgesailie Lake Series. PhD Thesis. McGill University 164pp.
- Muirhead, J.D., Kattenhorn, S.A., 2018. Activation of preexisting transverse structures in an evolving magmatic rift in East Africa. J. Struct. Geol. 106, 1–18.
- Muiruri, V.M., Owen, R.B., de Cort, G., McNulty, E., Rabideaux, N., Lowenstein, T., Renaut, R.W., Leet, K., Deocampo, D., Cohen, A.S., Campisano, C.J., Billingsley, A., Mbuthia, A., 2021. Middle Pleistocene to recent diatom floras and stratigraphy of the Magadi Basin, southern Kenya Rift. J. Paleolimnol. 65, 315–333.
- Njau, J.K., Toth, N., Schick, K., Stanistreet, I.G., McHenry, L.J., Stollhofen, H., 2020. The Olduvai Gorge Coring Project: drilling high resolution palaeoclimatic and palaeoenvironmental archives to constrain hominin evolution. Palaeogeogr. Palaeoclimatol. Palaeoecol. 110059.
- Owen, R.B., 2002. Sedimentological characteristics and origins of diatomaceous deposits in the east african rift system. In: Renaut, R.W., Ashley, G. (Eds.), Sedimentation in Continental Rifts, vol. 73. SEPM Spec. Publ., pp. 233–246
- Owen, R.B., Muiruri, V.M., Lowenstein, T.K., Renaut, R.W., Rabideaux, N., Luo, S., Deino, A.L., Sier, M.J., Dupont-Nivet, G., McNulty, E.P., Leet, K., Cohen, A.S., Campisano, C., Deocampo, D., Shen, C.-C., Billingsley, A., Mbuthia, A., 2018. Progressive aridification in East Africa over the last half million years and implications for human evolution. Proc. Natl. Acad. Sci. Unit. States Am. 115 (44), 11174—11179.
- Owen, R.B., Potts, R., Behrensmeyer, A., Ditchfield, P., 2008a. Diatomaceous sediments and environmental change in the Pleistocene Olorgesailie Formation, southern Kenya rift valley. Palaeogeogr. Palaeoclimatol. Palaeoecol. 269, 17–37.

- Owen, R.B., Renaut, R.W., Hover, V.C., Ashley, G.M., Muasya, A.M., 2004. Swamps, springs and diatoms: wetlands of the semi-arid Bogoria-Baringo Rift, Kenya. Hydrobiologia 518, 59–78.
- Owen, R.B., Renaut, R.W., Jones, B., 2008b. Geothermal diatoms: a comparative study of floras in hot spring systems of Iceland, New Zealand, and Kenya. Hydrobiologia 610, 175–192.
- Owen, R.B., Renaut, R.W., Muiruri, V.M., Rabideaux, N.M., Lowenstein, T.K., McNulty, E.P., Leet, K., Deocampo, D., Luo, S., Deino, A.L., Cohen, A., Sier, M.J., Campisano, C., Shen, C.-C., Billingsley, A., Mbuthia, A., Stockhecke, M., 2019. Quaternary history of the lake Magadi Basin, southern Kenya rift: tectonic and climatic controls. Palaeogeogr. Palaeoclimatol. Palaeoecol. 518, 97—118.
- Parkinson, J., 1914. The East African Trough in the neighbourhood of the soda lakes. Geogr. J. 44, 33–46.
- Potts, R., 1998. Environmental hypotheses of hominin evolution. Am. J. Phys. Anthropol. 107, 93–136.
- Potts, R., 2013. Hominin evolution in settings of strong environmental variability.

 Ouat. Sci. Rev. 73, 1–13.
- Potts, R., Behrensmeyer, A.K., Faith, J.T., Tryon, C.A., Brooks, A.S., Yellen, J.E., Deino, A.L., Kinyanjui, R., Clark, J.B., Haradon, C., Levin, N.E., Meijer, H.J.M., Veatch, E.G., Owen, R.B., Renaut, R.W., 2018. Environmental dynamics during the onset of the middle stone age in eastern Africa. Science 360, 86–90.
- Potts, R., Dommain, R., Moerman, J.W., Behrensmeyer, A.K., Deino, A.L., Beverly, E.J., Brown, E.T., Deocampo, D., Kinyanjui, R., Lupien, R., Owen, R.B., Rabideaux, N., Riedl, S., Russell, J.M., Stockhecke, M., deMenocal, P., Tyler Faith, J., Garcin, Y., Noren, A., Scott, J.J., Western, D., Bright, J., Clark, J.B., Cohen, A.S., Heil, C.W., Keller, C.B., King, J., Levin, N.E., Shannon, K.B., Muiruri, V., Renaut, R., Rucina, S.M., Uno, K., 2020. Increased ecological resource variability during a critical transition in hominin evolution. Sci. Adv. 6 (43), eabc8975. https://doi.org/10.1126/sciadv.abc8975.
- Potts, R., Faith, J.T., 2015. Alternating high and low climate variability: the context of natural selection and speciation in Plio-Pleistocene hominin evolution. J. Hum. Evol. 87. 5–20.
- Railsback, L.B., Gibbard, P.L., Head, M.J., Voarintsoa, N.R.G., Toucanne, S., 2015. An optimized scheme of lettered marine isotope substages for the last 1.0 million years, and the climatostratigraphic nature of isotope stages and substages. Quat. Sci. Rev. 111. 94–106.
- Renaut, R.W., Owen, R.B., Lowenstein, T.K., De Cort, G., McNulty, E., Scott, J.J., Mbuthia, A., 2021. The role of hydrothermal fluids in sedimentation in saline alkaline lakes: new evidence from Nasikie Engida, Kenya Rift Valley. Sedimentology 68, 108–134.
- Richardson, J., Dussinger, R., 1986. Paleolimnology of mid-elevation lakes in the Kenya rift valley. Hydrobiologia 143, 167–174.
- Richardson, J.L., Harvey, T.J., Holdship, S.A., 1978. Diatoms in the history of shallow East African lakes. Pol. Arch. Hydrobiol. 25, 341–353.
- Richardson, J.L., Richardson, A.E., 1968. Diatoms and Lake typology in East and central Africa. Int. Rev. Hydrobiol. 53, 299–338.
- Roubeix, V., Chalié, F., Gasse, F., 2014. The diatom *Thalassiosira faurii* (gasse) hasle in the ziway—shala lakes (Ethiopia) and implications for paleoclimatic reconstructions: case study of the glacial—holocene transition in East Africa. Palaeogeogr. Palaeoclimatol. Palaeoecol. 402, 104—112.
- Sepulchre, P., Ramstein, G., Fluteau, F., Schuster, M., Tiercelin, J.-J., Brunet, M., 2006. Tectonic uplift and eastern Africa aridification. Science 313, 1419–1423.
- Surdam, R.C., Eugster, H.P., 1976. Mineral reactions in the sedimentary deposits of the Lake Magadi region, Kenya. Geol. Soc. Am. Bull. 87, 1739–1752.
- Telford, R., Lamb, H., 1999. Diatom-derived palaeoconductivity estimates for Lake Awassa, Ethiopia: evidence for pulsed inflows of saline groundwater. J. Paleolimnol. 21, 409–422.
- ter Braak, C.J.F., 1986. Canonical correspondence analysis: a new eigenvector method for multivariate direct gradient analysis. Ecology 67, 1167–1179.
- Tziperman, E., Gildor, H., 2003. On the mid-Pleistocene transition to 100-kyr glacial cycles and the asymmetry between glaciation and deglaciation times. Paleoceanography 18, 1001 https://doi:10.1029/2001PA000627.
- Washbourn-Kamau, C.K., 1977. The Ol njorowa Gorge, Lake Naivasha basin, Kenya. In: Greer, D.C. (Ed.), Desertic Terminal Lakes. Utah Water Research Laboratory, pp. 297–307.
- Wohlenberg, J., Bhatt, N., 1972. Report on aeromagnetic surveys of two areas in the Kenya rift valley. Tectonophysics 15, 143–149.
- Zalat, A., Servant-Vildary, S., 2007. Environmental change in Northern Egyptian Delta lakes during the late Holocene, based on diatom analysis. J. Paleolimnol. 37, 273–299.